

INVESTIGATION ON LIFT AND DRAG COEFFICIENTS OF PROJECTILES AT VARIOUS ANGLES OF ATTACK



A THESIS SUBMITTED BY MD. RAFIQR RAHMAN

FOR THE DEGREE OF MASTER OF SCIENCE IN

MECHANICAL ENGINEERING

July 2020

DEPARTMENT OF MECHANICAL ENGINEERING

MILITARY INSTITUTE OF SCIENCE AND TECHNOLOGY

MIRPUR CANTONMENT, DHAKA - 1216, BANGLADESH.

The thesis titled “Investigation on Lift and Drag Coefficients of Projectiles at various angles of attack, Submitted by Md Rafiqur Rahman, Roll No: 101718002, Session: April 2017, has been accepted as satisfactory in partial fulfillment of the requirement for the degree of Master of Science in Mechanical Engineering on July 2020.

Board of Examiners

Professor Dr. Md. Quamrul Islam

Mechanical Engineering Department
MIST Dhaka-1216, Bangladesh

**Chairman
(Supervisor)**

Professor Dr. Mohammad Mamun

Mechanical Engineering Department
BUET Dhaka-1000, Bangladesh

**Member
(Co-Supervisor)**

Professor Dr. Dipak Kanti Das

Mechanical Engineering Department
MIST, Dhaka-1216, Bangladesh

Member

Col Md. Humayun Kabir Bhuiyan, psc

Mechanical Engineering Department
MIST Dhaka-1216, Bangladesh

**Member
(Ex Officio)**

Professor Dr. Mohammad Ali

Mechanical Engineering Department
BUET, Dhaka-1000, Bangladesh

**Member
(External)**

Declaration

I hereby declare that this thesis is my original work and it has been written by me.

I have duly acknowledged all the sources of information that have been used in the thesis. This thesis has also not been submitted for any degree in any university previously.

.....

Md. Rafiqur Rahman

July 2020

Acknowledgments

I am grateful to Almighty Allah for the successful completion of this research work. I would also like to express my gratefulness to Professor Dr. Md. Quamrul Islam, Department of Mechanical Engineering, MIST for his encouragement and invaluable advice in guiding and supervising. His sincere and to the point suggestions are gratefully acknowledged. I am humbly grateful to Professor Dr. Mohammad Mamun, Department of Mechanical Engineering, BUET for his valuable advice during several phases of this problem. I would like to express my special thanks to Colonel Md. Humayun Kabir Bhuyan, psc, Head, Department of Mechanical Engineering, MIST, Dhaka, for his great assistance in constructing the wind tunnel for the experiment. Finally, I would like to express my sincere thanks to all the general staff, lab assistants, and machine shop staff of the Mechanical Engineering Department for their cooperation and help in the successful completion of the work.

List of Contents

Title	i
Signature	ii
Declaration	iii
Acknowledgments	iv
List of Contents	v
Abstract	vii
Nomenclature	viii
List of Figures	ix
List of Tables	xi
1. Introduction	
1.1. General	1
1.2. Background of the study	2
1.3. Problem statement	3
1.4. Aerodynamic Study	3
1.4.1. Drag	3
1.4.2. Types of drag	4
1.4.3. Drag coefficient	4
1.4.4. Lift force	6
1.4.5. Lift coefficient	7
1.4.6. Mathematical theories of lift	8
1.4.7. Angle of attack	8
1.4.8. Pressure coefficient	9
1.5. Necessity of study	10
1.6. Requirement of model study	11
1.7. Objective of this research	12

2. Literature Review	
2.1. General	13
2.2. Existing work on aerodynamic characteristics	13
3. Experimental Setup	
3.1. General	23
3.2. Experiment	23
3.3. Preparation of the Woden Model	24
3.4. Wind Tunnel	27
3.5. Test Section	29
3.6. Measuring Equipment	30
3.7. Experimental Conditions	30
4. Mathematical Model and Simulation	
4.1. Mathematical Model	31
4.2. Determination of Pressure Coefficient	32
4.3. Determination of Drag and Lift Coefficient	33
4.4. Geometrical setup	36
4.5. Simulation and Mesh Settings	38
5. Results and Discussion	43
6. Conclusions and Recommendation	63
7. Reference	66
8.1 Appendix A Inclined Multi-Manometer reading of 37 mm Projectile	72
8.2 Appendix B Inclined Multi-Manometer reading of 57 mm Projectile	73
8.3 Appendix C Inclined Multi-Manometer reading of 125 mm Projectile	74
8.4 Appendix D Inclined Multi-Manometer reading of 57 mm projectile in Oblique Angles	75

ABSTRACT

Improvement in terminal accuracy is an important objective for future artillery projectiles. Generally, it is often associated with range extension and precision. This paper deals with the research of aerodynamic characteristics of anti-aircraft artillery and medium tank projectiles. In Bangladesh, a very little study is available for determining the aerodynamic characteristics of projectiles which are used in the Bangladesh army. When a projectile is launched it experiences a drag force which is more than the gravitational force due to the supersonic speed of the projectile. Aerodynamic characteristics are strictly related and will affect the stability of the projectiles, thus it is vital to obtain reliable aerodynamic characteristics estimation to carry out a good design of projectile. In this study, a set of a hollow projectile is considered since it shows good performance characteristics and it is easy to handle. For our research we have considered two types of anti-aircraft artillery projectiles, i.e. 57 mm & 37 mm and 125 mm medium tank projectile. Both experimental and numerical studies have been done on this type of projectiles. In this study, the main emphasis is given to determine the pressure coefficient, Drag coefficients, lift coefficient, and the behavior pattern of the projectiles at different angles of attack. To study the aerodynamic characteristics of the projectiles the experiment is conducted in an open circuit subsonic wind tunnel available at MIST where uniform flow velocity (4.7m/s) is maintained across the flow direction. For the experiment, the angle of attack is varied between 30° to 50° is considered with an interval of 5°. Here inclined manometer was used to find out the surface static pressure and then the pressure coefficient was determined from that. Finally, for the numerical scheme, the ANSYS Software was used to simulate the experiment. In this study, it was found that the drag and lift forces acting on the projectiles, increase with the increase in the size. In some cases, the drag and lift forces increase by more than 80%. The drag and lift forces also increased when the angle of attack increases. However, it was found that the rate of increasing the lift forces is higher (45%) than the drag forces for a case.

NOMENCLATURE

Symbol	Description (Units)
C_P	<i>Pressure Coefficient (Unit less)</i>
C_D	<i>Drag Coefficient (Unit less)</i>
C_L	<i>Lift Coefficient (Unit less)</i>
L_D	<i>Drag Force (N)</i>
L_L	<i>Lift Force (N)</i>
P	<i>Static Pressure On the Projectile (Pa)</i>
P_∞	<i>Ambient Pressure (Pa)</i>
Δl_k	<i>Manometer Height Difference (m)</i>
F	<i>Total Force (N)</i>
ρ_k	<i>Density of Manometer Fluid (Kg/m³)</i>
ρ_{air}	<i>Density of Air (Kg/m³)</i>
U_∞	<i>Air Velocity (m/s)</i>
α	<i>The Angle of Attack (AOA) (°)</i>
g	<i>Gravitational Acceleration (m/s²)</i>
F_1	<i>Force Acting on Projected Area '1' (N)</i>
S_{Total}	<i>Total Active Projected Area (m²)</i>

List of Figures

Figures	Page Number
Figure 1: Aerodynamic Force	6
Figure 2: Angle of attack	8
Figure 3: 3D model of the 57 mm projectile	24
Figure 4: Model Wooden of the Projectile	25
Figure 5: Various projectiles	25
Figure 6: Tapping positions are shown on the cross-section of projectiles	26
Figure 7: Experimental setup of 57 mm projectile for measuring static pressure.	27
Figure 8: Schematic diagram of a wind tunnel	28
Figure 9. Wooden Projectiles Manufactured.	31
Figure 10: Plane view of the Projectile form air direction	35
Figure 11: Area has drawn from the projection of the segments.	35
Figure 12: Measurement of the projected area.	36
Figure 13. Geometry files for CFD simulation (a) 37 mm, (b) 57 mm, and (c) 125 mm Projectiles.	38
Figure 14: Mesh of the CFD Simulation for (a) 37 mm, (b) 37 mm (zoomed) Projectiles.	41
Figure 15: Mesh of the CFD Simulation for (a) 57 mm, and (b) 125 mm Projectiles.	42
Figure 16 : Ansys CFD Simulation setting for (a) 37mm, (b) 57 mm, and (c) 125 mm projectile.	44
Figure 17: Angle of Attack vs Drag Force.	47
Figure 18: Angle of Attack vs Lift Force.	48
Figure 19: Angle of Attack vs Drag Coefficients.	50
Figure 20: Angle of Attack vs Lift Coefficients.	51
Figure 21: Tapping Point Vs Pressure Coefficients for 37 mm Projectile.	53
Figure 22: Tapping Point Vs Pressure Coefficients for 57 mm Projectile.	53

Figure 23: Tapping Point Vs Pressure Coefficients for 125 mm Projectile.	54
Figure 24: The pressure contour for 37 mm projectile at 45°AOA.	55
Figure 25: The velocity contour for 37 mm projectile at 45°AOA.	55
Figure 26: The pressure contour for 57 mm projectile at 45° AOA.	56
Figure 27: The velocity contour for 57 mm projectile at 45°AOA.	56
Figure 28: The pressure contour for 125 mm projectile at 45°AOA.	57
Figure 29: The velocity contour for 125 mm projectile at 45°AOA.	57
Figure 30: The lift and drag coefficient of 57 mm projectile at 45° AOA for supersonic speed.	58
Figure 31: The rotation of the 57mm projectile at different angles	60
Figure 32: The projected area for (a) Side (b) 45 Degree Left, and (C) Back	61
Figure 33: Forces acting on the Projectile at different 45° at a different orientation	64

List of Tables

Tables	Page Number
Table 1: Experimental Conditions for Different Projectiles.	30
Table 2: Grid Independency Test	39
Table 3: Simulation and Experimental Drag Forces on 37, 57, and 125 mm Projectiles at Different AOA.	47
Table 4: Simulation and Experimental Lift Forces on 37, 57, and 125 mm Projectiles at Different AOA	47
Table 5: Simulation and Experimental Drag Coefficients on 37, 57, and 125 mm Projectiles at Different AOA	50
Table 6: Simulation and Experimental Lift Coefficients on 37, 57, and 125 mm Projectiles at Different AOA	50
Table 7: Total acting forces on 57 mm Projectile at 45° attack angle and for different orientations.	62

CHAPTER-1

INTRODUCTION

1.1 General

In the primitive age, the first stone hurled by prehistoric man was probably the earliest example of external ballistics. The advantages of being able to throw farther and with more power led to devices such as slings and spears. The bow is an extension of it called the “ballista” from which ballistics derives its name. It was the work of Leonardo da Vinci which led to the early development of modern ordnance engineering. He designed many kinds of weapons, both offensive and defensive, ranging from cannonballs, mortars, rifled firearms, up to primitive versions of the tank, and submarine. Da Vinci was also the first to provide a theoretical basis for the phenomena of aerodynamics. Later Leonhard Euler of Switzerland analyzed the results of experimental range firings to determine the drag on cannonballs. He investigated drag at low and high velocities.

Accurate experimental methods for determining the drag of the projectile is very important. The trajectory of a projectile through the air is affected both by gravity and by aerodynamic forces. The aerodynamic forces can conveniently be ignored in many situations, even when they are comparatively large. When a projectile is launched it experiences a drag force which is more than the gravitational force. The trajectory of a projectile is strongly affected by the drag force. More dramatic changes in the trajectory of a projectile occur when the projectile is relatively light and when the gravitational force is significantly smaller than the lift and drag forces.

1.2 Background of the study

Drag and lift coefficients play a vital role in projectile flight. These coefficients depend on the angles of attack, the nose shape of the projectile, velocity, and surface smoothness. However, the drag experienced by a single projectile will be different from the drag force experienced by two projectiles flying side by side since the disturbance created in the flow field by one projectile will affect the other one. Drag is the prime reason for reducing projectile velocity and accuracy. Thus it is necessary to determine and minimize the effect of drag to improve the range of projectiles.

Total drag has three components namely, (i) pressure, (ii) skin friction, and (iii) base drag among which one or two components become dominant at different speed levels. Since projectiles like different ammunition shells operate at a different speed (subsonic and supersonic) this breakdown will aid the designer to find potential areas for drag reduction and achieve the desired increase in range.

Research on hollow projectile has increased nowadays for its good performance characteristics like superior target penetration, inexpensive manufacturing, low recoil, and easy handling. Both experimental and numerical studies are done on this type of projectile. Good agreements between numerical results and experimental observations are obtained where the coefficient of drag obtained at different Mach numbers was used for estimation of trajectory elements for the supersonic projectile. However, a very little study is available for the drag coefficient for projectiles flying side by side.

In this investigation, the static measurements of coefficients and gradient of aerodynamic force and moments depending on Mach number and angle of attack in the subsonic wind tunnel are done on the symmetric projectile. Optimization of the structural design and micro correction projectile aerodynamic shape is investigated.

1.3 Problem statement

In modern warfare, the design of the projectiles is largely focused on its range and accuracy. Aerodynamics forces have a huge impact on the trajectory of a projectile. The influence Parameters for the estimation of trajectory elements are drag Coefficients, lift Coefficients, angles of attack, muzzle velocity, atmospheric conditions, and the projectile shape and size. Given the view, we have considered three different types of Projectiles i.e 57 mm, 37 mm anti-aircraft, and 125 mm tank projectiles in the present study to emphasis on determining the following parameters:

- i) Drag force and Drag Coefficient at various angles of attack.
- ii) Lift force and Lift Coefficient at various angles of attack.
- iii) Pressure Coefficient for each tapping point needs to be determined from the surface static pressure.

1.4 Aerodynamic Forces

1.4.1 Drag

In fluid dynamics, drag (sometimes called air resistance, a type of friction, or fluid resistance, another type of friction or fluid friction) is a force acting opposite to the relative motion of any object moving with respect to a surrounding fluid. This can exist between two fluid layers (or surfaces) or a fluid and a solid surface. Unlike other resistive forces, such as dry friction, which are nearly independent of velocity, drag forces depend on velocity. Drag force is proportional to the velocity for a laminar flow and the squared velocity for a turbulent flow. Even though the ultimate cause of a drag is viscous friction, the turbulent drag is independent of viscosity. Examples of drag include the component of the net aerodynamic or hydrodynamic force acting opposite to the direction of movement of a solid object such as projectiles, aircraft, cars, and so on.

1.4.2 Types of drag

Types of drag are generally divided into the following categories:

i) Form drag (Pressure drag)

Form drag known also as pressure drag arises because of the shape and size of the object. The pressure drag is proportional to the difference between the pressures acting on the front and back of the immersed body, and the frontal area. This type of drag force is also an interesting consequence of the Bernoulli's effect. According to Bernoulli's principle, faster-moving air exerts less pressure.

ii) Skin friction drag

Skin friction drag is a component of profile drag, which is a resistant force exerted on an object moving in a fluid. Skin friction drag is caused by the viscosity of fluids and is developed from laminar drag to turbulent drag as a fluid moves on the surface of an object. Skin friction drag is generally expressed in terms of the Reynolds number, which is the ratio between inertial force and viscous force.

iii) Base drag

Drag which is generated in an object moving through fluid from the shape of its rear side

1.4.3 Drag Coefficient

In fluid dynamics, the drag coefficient is a dimensionless quantity that is used to quantify the drag or resistance of an object in a fluid environment, such as air or water. It is used in the drag equation in which a lower drag coefficient indicates the object will have a less aerodynamic or hydrodynamic drag. The drag coefficient is always associated with a particular surface area. The drag coefficient of any object comprises the effects of the two basic contributors to fluid dynamic drag that is skin friction and form drag. The drag coefficient of a lifting airfoil or hydrofoil also includes the effects of lift-induced drag. The

drag coefficient of a complete structure such as a projectile also includes the effects of interference drag.

The drag coefficient C_d is defined as

$$C_d = \frac{2L_d}{\rho_\infty U_\infty^2 A}$$

Where F_d is the drag force, which is by definition the force component in the direction of the flow velocity,

where

ρ_∞ = Mass density of the fluid,

U_∞ = Flow speed of the object relative to the fluid,

A = Reference area.

The reference area depends on what type of drag coefficient is being measured. For automobiles and many other objects, the reference area is the projected frontal area of the vehicle. This may not necessarily be the cross-sectional area of the vehicle, depending on where the cross-section is taken. For example, for a sphere $A = \pi r^2$ (note this is not the surface area $= 4\pi r^2$). The Drag Coefficient (C_d) is not a constant but varies as a function of flow speed, flow direction, object position, object size, fluid density, and fluid viscosity. Speed, kinematic viscosity, and a characteristic length scale of the object are incorporated into a dimensionless quantity called the Reynolds Number (Re). The Drag Coefficient (C_d) is thus a function of the Reynolds Number. In a compressible flow, the speed of sound is relevant, and the drag coefficient is also a function of Mach number (Ma).

1.4.4 Lift Force

A fluid flowing around the surface of an object exerts a force on it. Lift is the component of this force that is perpendicular to the oncoming flow direction. It contrasts with the drag force, which is the component of the force parallel to the flow direction. Lift conventionally acts in an upward direction to counter the force of gravity, but it can act in any direction at right angles to the flow shown in Figure 1.

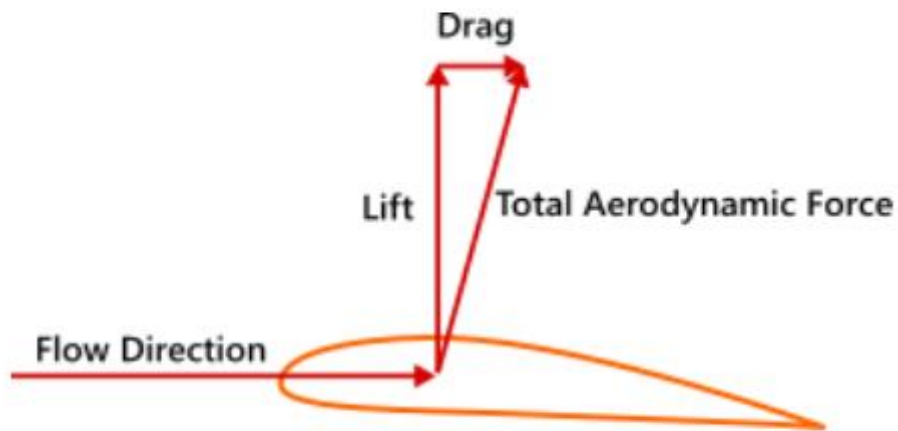


Figure 1: Aerodynamic Force

Lift is defined as the component of the aerodynamic force that is perpendicular to the flow direction, and drag is the component that is parallel to the flow direction. A fluid flowing around the surface of an object applies a force against it. It makes no difference whether the fluid is flowing past a stationary body or the body is moving through a stationary volume of fluid.

Lift is mostly associated with the wings of fixed-wing aircraft, although it is more widely generated by many other streamlined bodies such as propellers, kites, helicopter rotors, racing car wings, maritime sails, and wind turbines in air, and by sailboat keels, ship's rudders, and hydrofoils in water. Lift is also exploited by flying and gliding animals, especially by birds, bats, and insects, and even in the plant world by the seeds of certain trees.

While the common meaning of the word "lift" assumes that lift opposes weight, the lift can be in any direction with respect to gravity, since it is defined with respect to the direction of flow rather than to the direction of gravity.

1.4.5 Lift coefficient

The lift coefficient (C_L) is a dimensionless coefficient that relates the lift generated by a lifting body to the fluid density around the body, the fluid velocity, and an associated reference area. A lifting body is a foil or a complete foil-bearing body such as a fixed-wing aircraft. C_L is a function of the angle of the body to the flow, its Reynolds number, and its Mach number. The lift coefficient C_L refers to the dynamic lift characteristics of a two-dimensional foil section, with the reference area replaced by the foil chord. The lift coefficient C_L is defined by

$$C_L = \frac{2L}{\rho u^2 S}$$

If the value of C_L for a wing at a specified angle of attack is given, then the lift produced for specific flow conditions can be determined:

where

L = Lift force

ρ = Air Density

U = Velocity or true airspeed

S = Projected wing area

C_L = Lift coefficient at the desired angle of attack, Mach number, and Reynolds number

1.4.6 Mathematical theories of lift

Mathematical theories of lift are based on continuum fluid mechanics, assuming that air flows as a continuous fluid. Lift is generated per the fundamental principles of physics, the most relevant being the following three principles:

i) Conservation of momentum

Which is a consequence of Newton's laws of motion, especially Newton's second law which relates the net force on an element of air to its rate of momentum change,

ii) Conservation of mass

Including the assumption that the airfoil's surface is impermeable for the air flowing around,

iii) Conservation of energy

Which says that energy is neither created nor destroyed.

1.4.7 Angle of attack



Figure 2: Angle of attack

The angle of attack is the angle between the chord line of an airfoil and the oncoming airflow shown in Figure 2. A symmetrical airfoil will generate zero lift at zero angle of attack. But as the angle of attack increases, the air is deflected through a larger angle, and the vertical component of the airstream velocity increases, resulting in more lift. For small angles, a symmetrical airfoil will generate a lift force roughly proportional to the angle of attack.

As the angle of attack increases, the lift reaches a maximum at some angle; increasing the angle of attack beyond this critical angle of attack causes the upper-surface

flow to separate from the wing; there is less deflection downward so the airfoil generates less lift. The airfoil is said to be stalled.

1.4.8 Pressure coefficient

A pressure coefficient is a dimensionless number that describes the relative pressures throughout a flow field in fluid dynamics. The pressure coefficient is used in aerodynamics and hydrodynamics. Every point in a fluid flow field has its unique pressure coefficient, C_p .

In many situations in aerodynamics and hydrodynamics, the pressure coefficient at a point near a body is independent of body size. Consequently, an engineering model can be tested in a wind tunnel or water tunnel.

The pressure coefficient is a parameter for studying the flow of incompressible fluids such as water, and also the low-speed flow of compressible fluids such as air. The relationship between the dimensionless coefficient and the dimensional numbers is

$$C_p = \frac{P - P_\infty}{\frac{1}{2} \rho_\infty V_\infty^2}$$

where

'P' is the pressure at the point at which pressure coefficient is being evaluated

P_∞ is the pressure in the freestream (i.e. remote from any disturbance)

ρ_∞ is the freestream fluid density (Air at sea level and 15 °C is 1.225 kg/m³)

V_∞ is the freestream velocity of the fluid

In the fluid flow field around a body, there will be points having positive pressure coefficients up to one, and negative pressure coefficients including coefficients less than minus one, but nowhere will the coefficient exceed plus one because the highest pressure that can be achieved is the stagnation pressure. The only time the coefficient will exceed plus one is when advanced boundary layer control techniques, such as blowing, is used.

1.5 Necessity of the study

The requirement for the present study is to estimate numerically the Coefficient of drag & lift and shock wave pattern at different Mach numbers for anti-aircraft artillery Projectiles and also for 125 mm med tank projectile. Here the estimated drag & lift coefficient will be used as an input Parameter for the simulation of trajectory elements. Then the numerical results will be validated with experimental data. Finally, the comparison will be made with the estimated drag & lift coefficient of two projectile flying side by side.

The calculation of the projectile flow field has considerable importance for efficient design. The flow fields are very complex due to their mixed hyperbolic-elliptic nature, viscous effects, and their three-dimensionally as well. The complexities of three-dimensional viscous inlet flow make their numerical prediction a very difficult task. But still, in recent years the three-dimensional hollow projectile research development became very important for small calibers artillery projectile. The circular duct along with the longitudinal axis of the hollow projectile which causes high muzzle velocity and low drag makes its performance characteristics greatly improved.

In the aerodynamics property there are two basic parameters, namely, lift and drag which are very important for the design of an artillery projectile. There are many methods available for the simulation, however, to achieve more reliable results, wind tunnel test is usually recommended. The study is performed to develop a computational fluid dynamics (CFD) based method to predict longitudinal and lateral-directional aerodynamic Coefficients of projectiles. As aerodynamic characteristics are strictly related and will affect the stability of the projectile thus it is vital to obtain reliable aerodynamic characteristic estimation to carry out a good design of projectile. Again within the field of artillery lots of steps have been taken to increase the range and accuracy of the guns. The increase of the range can be achieved either by gun improvement, the increased gas

pressure in the barrel or by the improvements of projectile performance. Projectile performance largely depends on the aerodynamic characteristics.

In light of the above, the aerodynamics characteristics will have a direct impact on projectile stability, accuracy, and range. Thus the study is conducted and presented the result obtained from wind tunnel test experiments on different types of anti-aircraft artillery and 125 mm medium tank projectiles to study the pattern of their behavior at different angles of attack.

1.6 Requirement of Model study

There are roughly four classes of techniques to predict aerodynamic forces and moments on a projectile in atmospheric flight. These are empirical methods, wind tunnel testing, computational fluid dynamics simulation, and spark range testing. In computational fluid dynamic (CFD) simulations, the fundamental fluid dynamic equations are numerically solved for a specific configuration. Wind tunnels testing and full-scale results are always different due to Reynold's number inequality. In most of the wind tunnel test, the full-scale Reynolds number is difficult to achieve. Boundary layer separation depends on Reynold's number where for sharp-edged structures separation point does not depend on Reynolds number. On the other hand, the flow field around curved surfaces is very much Reynolds number dependent, so tests on these configurations must be treated with care. The crosswind scales in wind tunnels are often less-than reality. This can cause underestimation of crosswind effects. The scale difference between the wind tunnel model and prototype is found in the high-frequency fluctuation. High peaks found on the cladding in full-scale are not found in the wind tunnel. Those effects may be caused by structural details that are not simulated in the wind tunnel model.

For determining aerodynamic Coefficient data including the total aerodynamic drag and lift, studies with the model and full-scale projectile are performed to validate the

model. But full-scale experiments are both costly and difficult to perform. For the present study with anti-aircraft artillery and tank projectiles, full-scale experiments will not only be complex and costly but also it would be difficult to record reliable pressure distribution simultaneously on the single as well as a group of the projectile as there will be a variation of speeds and direction of the wind with time. The flow around projectile in the actual environment is very complex and formulation of a mathematical model to predict the flow is almost impossible. Thus for solution accuracy model study of anti-aircraft artillery & tank projectile and various data obtained from the simulation will become very handy for practical analysis.

1.7 Objective of this research

1.7.1 Objective with the specific aim

Experimental investigations will be carried out in the wind tunnel with the different types of hollow shape dummy anti-aircraft projectile i.e 37 mm, 57 mm, and 125 mm dummy medium tank projectiles. Specific objectives are as follows:

- i) To determine the drag and lift coefficient of projectiles of different sizes and nose shapes at various angles of attack while flying.
- ii) Numerical modeling of flow over various projectiles.
- iii) Recommendation for modification of existing anti-aircraft Artillery projectiles.

1.7.2 Possible outcome

The possible outcome of the study will hopefully help in future research work with artillery projectile in the following ways:

- i) Can be used for finding zero yaw coefficient of drag and trajectory elements of different Mach numbers for shells.
- ii) Aid in the inspection of range, terminal velocity, and striking energy of a given projectile.

CHAPTER-2

REVIEW OF LITERATURE

2.1 General

Drag and lift coefficients are very important components for the projectile flight and it poses a huge effect on the overall projectile aerodynamic characteristics, especially on its range and accuracy. So it is necessary to determine the effects of the aerodynamic forces i.e drag & lift forces and its coefficient on the projectile. Many studies and researches are performed in the past to study drag and lift coefficients for various types of projectiles. Some of the studies are carried out on aerodynamic characteristics to predict & improve its aerodynamic performance and some for improving the range & accuracy. All those researches are essential as any findings will help in the overall projectile's aerodynamic characteristics and its performances. Some of the important findings in a brief description of the related problem are highlighted in this chapter.

2.2 Existing work on aerodynamic characteristics

Mohammad Amin et al. [1] prepared an article that focused on the study of various methods for reducing the base drag of artillery projectiles caliber 122mm. The computational fluid dynamics (CFD) numerical simulations (RANS, 2-D axisymmetric configuration) were performed, to investigate the base drag characteristics of the projectiles, with various base shapes and different techniques to reduce the base drag coefficient at a different Mach number (from $M = 0.9$ to 2.2). Since the low pressure in the afterbody region during the projectile's flight, which is responsible for up to 50% of the total drag, therefore reducing the base drag is an efficient and practical way to reduce the total drag of the projectile.

Elsaadany et al. [2] investigate in their study the use of a drag brake module mounted on a spin-stabilized artillery projectile to correct range. To illustrate the effectiveness of the correction module, an accurate trajectories prediction via atmospheric

flight is demonstrated using a full six-degree-of-freedom nonlinear model. The model includes Earth's rotation and ellipsoidal shape. The computational flight analysis takes into consideration all the aerodynamics variations using the variable aerodynamic coefficients, in addition to gravity. The simulation results show that the impact accuracy of a conventional projectile using this drag brake module can be improved.

Mahfouz et al. [3] in their study applied computational fluid dynamics (CFD) to simulate a 2-D hollow projectile with optimal geometry at different Mach numbers at $1 < Ma < 1.8$ and different angles of attack to investigate the shock wave structures and drag characteristics. Different types of shock waves appear in the front of the projectile with the variation of Mach numbers, and the structures of flow fields and total drag coefficients have obvious differences. Moreover, the influences of the viscous effects on the pressure distribution of the projectile surface and total drag are analyzed. Finally, the variations of drag and lift coefficients with different Mach numbers and different angles of attack are discussed in detail.

Kiran et al. [4] Investigated in their research the aerodynamic properties of a standard M549, 155mm projectile. Aerodynamic data from wind tunnel and range testing was benchmarked against aerodynamic prediction and semi-empirical design codes like MCDRAG, NSWCAP, and Aero-Prediction. Further, they deal with the prediction of drag by benchmarking the results of standard M549 projectile design and predicting the boat tail angle effect for the different drag coefficient. The detailed study is done and validated to reduce drag and see its effect on the projectile design for both transonic and supersonic speeds.

Sarsar et al. [5] in their study applied various methods and modifications to correct the range and deflection of artillery projectile like impulse thruster, pulsejet, drag devices, reciprocating canards. Out of these methods, one is drag brake deployment which is analyzed in this paper. A trajectory corrector module consisting of the disc is placed at

the aft of the fuze. Once deployed, it increases the frontal area and hence the drag which reduces the overshoot range. Analysis has been carried out for increased frontal area, initiation, and duration of deployment and optimum range correction with a varying diameter of drag brakes using simulation.

Baranowski et al. [6] describe in their paper the process of identification of the mathematical model of spin-stabilized artillery projectile's motion in the atmosphere. The aerodynamic characteristics needed for the motion model are identified by using an artificially generated trajectory of projectile that imitates the flight path recorded by the 3D Doppler radar. The trajectories of 35 mm projectile were generated using the motion model with 6 degrees of freedom with the aerodynamic coefficients produced by PRODAS software. The identification process was conducted for the explicit form of the modified point-mass trajectory model. The main goal of the presented work is to obtain a valid tool for aerodynamic coefficients identification based on real data gathered during field tests.

M A Suliman et al. [7] conducted a computational investigation for the 155mm artillery shell to reduce the base drag. Three case studies were conducted to investigate the properties of the flow field around the shell for the flight at different Mach numbers at zero angles of attack. The three cases were: a shell with boat tail, a shell with a base cavity, and a shell with base bleed. Also, combinations of these three cases were investigated. The higher drag reduction was demonstrated when using a combination of the three effects. For this latter case, it was possible to realize a drag coefficient reduction of ~60% at the subsonic regime and ~20-30% at transonic and supersonic regimes.

Alexander [8] shows in his work, that increasing the range of the shells and bullets 2-5 times can be made by including small wings. The shell/bullet specially formed wings to support the projectile in the air, does not allow it to fall in earth's surface as the kinetic energy of the projectile is not fighting the forces of gravity and air resistance. This is an

important innovation as it can be used in conventional rifles and guns with a rifled barrel and rotary shell/bullet. The second idea is a radical change in trajectory. The projectile reaches high altitudes and glides from height using wings with subsonic speed and at a good ratio of lift/drag. The author developed a theory of these projectiles and computed some projects which show the high efficiency of these innovations.

Chand et al. [9] discussed in their paper the feasibility of the application of the system dynamics approach in the artillery projectile motion analysis under the test and evaluation curriculum activities using a point-mass mathematical model concept by assuming acted upon by gravity and aerodynamic drag, acting in the opposite direction. The model requires only a limited amount of data, namely, one aerodynamic a parameter (C_D) as a function of Mach number, the projectile mass & diameter, and simple launch parameters. The resulting equations of motion have been numerically solved to yield the complete trajectory elements of a projectile.

Goran et al. [10] present the modification of the existing guided missile in their study. The modification was performed based on required aerodynamic coefficients for the existing guided missile. The preliminary aerodynamic configurations of the improved missile front parts were designed based on theoretical and computational fluid dynamics simulations. All aerodynamic configurations were tested in the T-35 wind tunnel to determine the final geometry of the new front parts. The computational results of the aerodynamic loads of a guided missile model are also given and agreed well with.

Liang et al. [11] discussed in their paper, some fundamental studies on the structural and aerodynamics features for the guided projectile in the preliminary design of its exterior ballistics. It studied the aerodynamic characteristics of different kinds of trajectory correction projectiles. They provided some helpful references to investigate the aerodynamic characteristics in the preliminary design. An optimal design method was

developed in this paper to obtain the aerodynamic parameters of the control canards for trajectory correction.

Chand et al. [12] set an objective in their present study to propose a single mathematical model to estimate the trajectory elements of a typical 105 mm artillery projectile, using the concept of simplified point-mass model, which is validated through the Doppler DR-5000 measurements. In this study, the influence parameters such as muzzle velocity, angle of inclination, drag coefficient, atmospheric conditions, and projectile shape & size have been considered for estimation of trajectory elements.

Ahmed [13] described in his paper the determination of aerodynamic coefficients by shell designers is a critical step in the development of artillery projectile design, of particular interest, is the determination of the aerodynamic coefficients at transonic speeds. In his work, a solution algorithm based on finite-difference MacCormack's technique is used for solving mixed subsonic-supersonic flow problems. Details of the asymmetrically located shock waves on the projectiles have been determined. The pitching moment coefficient, determined from the computed flow fields, shows the critical aerodynamic behavior observed in free flights.

Sahoo et al. [14] in their study, made a numerical estimation of the drag variation and trajectory elements of a supersonic projectile having two different nose shapes. The study aims at finding the coefficient of drag and shock wave pattern for 130 mm artillery shell fitted with recovery plug or with fuze when traveling at zero angles of attack in the supersonic flow of air. The coefficient of drag (C_D) obtained from the simulation is used as an input parameter for the estimation of trajectory elements. The numerical results, i.e, the coefficient of drag at different Mach numbers and trajectory elements are validated with the data recorded by tracking radar from an experimental firing.

Elya et al. [15] present in their paper an experimental test of the broadly applied framework that employs supersonic drag coefficients that are independent of air density.

Experimental drag coefficients are usually calculated when the other factors are measured experimentally. To test the theoretical relationship between drag force and air density at supersonic speeds, a 2.59 g projectile was launched at six different velocities between Mach 1.2 and Mach 2.9 and two air densities.

Jian et al. [16] in their analysis shows a hypersonic aerodynamics analysis of an electromagnetic gun launched projectile configuration is undertaken to ameliorate the basic aerodynamic characteristics in comparison with the regular projectile layout. With a steady-state computational fluid dynamics (CFD) simulation, the basic density, pressure, and velocity contours of the EM gun projectile flow field at Mach number 5.0, 6.0, and 7.0 (angle of attack= 0°) have been analyzed. Drag, lift, and pitch property variations are all illustrated with the changes of Mach number and angle of attack. The results show that the configuration optimized projectile, launched from the EM gun at Mach number 5.0 to 7.0, acts in a much more stable way than the projectiles with the regular aerodynamic layout.

Jasminder et al. [17] show in their study that NACA (national advisory committee for aeronautics) airfoils have been generated according to the NACA standards. The effects of fluid flow have been studied over the two airfoils 4412 and S1223 through computational fluid dynamics. The comparison was done on the basis coefficient of lift and coefficient of drag. The angle of attack was varied and their effect was seen on velocity, pressure, coefficient of lift, and coefficient of drag.

Shane [18] defined in his project what drag force is, derived the governing equation for drag and listed some applications of drag forces. Derivation of the drag equation was achieved using the Buckingham π theorem, a dimensional analysis tool. Lastly, this project explored the problem of how long and how far a dragster takes to stop once the projectile is deployed.

Shubham et al. [19] presented in their paper steady-state, two-dimensional computational investigations performed on NACA 0012 airfoil to analyze the effect of variation in Reynolds number on the aerodynamics of the airfoil without and with a Gurney flap. RANS based one-equation Spalart-Allmaras model is used for the computations. Both lift and drag coefficients increase with Gurney flap compared to those without Gurney flap at all Reynolds numbers at all angles of attack. The zero-lift angle of attack seems to become more negative as Reynold's number increases due to the effective increase of the airfoil camber.

Wenjun et al. [20] in their study investigated the aeroelastic influences on the aerodynamic performance and flight stability of a large length to diameter ratio projectile, free-flight experiments on both the flexible and rigid projectile model. The projectile flight velocity, angle of attack, and precision are obtained after the data procession. Moreover, the aerodynamic force and moment coefficients of two kinds of projectiles are presented, their aerodynamic performances and flight stability are compared and analyzed. Results show that the flexible projectile has a larger drag coefficient than the rigid.

Peter [21] in his paper shows an analytic approach for the investigation of the projectile motion in a medium with quadratic resistance. The objective of the present work is to give simple formulas for the construction of the projectile trajectories under the motion with quadratic air resistance that is drag force.

Mariusz et al. [22] presented the results of a comparison between drag coefficients established by the firing tests and numerical simulations in the paper. The results of numerical calculations carried out by the CFD method, exploiting Ansys Fluent v16 software. Required range may be achieved both by the increase of the muzzle velocity and the application of a new projectile shape to get lower coefficients of drag.

Hossam [23] introduces the area of projectile range extension with different concepts and methods in his paper. Three main methods of range increase were selected

among all the reviewed ones. The first is drag reduction by base bleeding, in which both a mathematical model and computational work are used to investigate the ballistic performance of a projectile with live base bleed.

Damir et al. [24] show in this paper the research of aerodynamic characteristics of classic symmetric projectile. Based on constructed parameters and dynamic characteristics of the 40 mm projectile model it calculates aerodynamic coefficients and their derivatives. It performs the static measurements of coefficients and gradients of aerodynamic forces and moments depending on Mach number and angle of attack, in the three-sonic wind tunnel. Utilizing wind tunnel flow visualization chart and numerical results of aerodynamic coefficient the comparative analysis is made and the accuracy of aerodynamic characteristics is evaluated.

Tong et al. [25] in their paper aiming to research aerodynamic characteristics of mortar projectiles. This paper builds three simulation models with fins in different amount and appearance, to generate meshes of each model, it simulates the changing laws of drag coefficient, lifts coefficient according to the data. Simulation results indicate that projectile with folded fins have a better aerodynamic appearance and it provides an aerodynamic reference for future research.

Jiemin et al. [26] researched the aerodynamic characteristics of a two-dimensional trajectory correction fuze used for the common artillery ammunition, which increases the targeting accuracy by decreasing the circular error probability. In their study, computational fluid dynamic (CFD) simulation is performed to study the aerodynamic characteristics of the trajectory correction fuze. Calculation covered from -10 to 10 degrees steering canard deflection over a speed range from Mach 0.6 to 3.

Jan et al. [27] made a numerical study to analyze the performance of a secant-ogive-cylinder projectile in the transonic regime in terms of aerodynamic drag. At transonic speeds, the base drag contributes a major portion of the total aerodynamic drag

and hence affects projectile's performances significantly. The base bleed method is applied to reduce the base drag by varying the value of parameters, the bleed quantity (l), and the bleed area ratio (ω). At Mach number 0.96, the reductions in base drag and total drag can be as high as 64% and 44%, respectively, for $l = 0.1$ and $\omega = 0.3$.

Hruschka et al. [28] analyzed in their paper, the transient shock dynamics and drag characteristics of a projectile flying through a pipe at transonic speed using time-of-flight and pipe wall pressure measurements as well as computational fluid dynamics (CFD). When projectile speed and hence compressibility effects are low, the presence of the pipe has little influence on the drag.

Chun et al. [29] adopted computational fluid dynamics (CFD), low-speed wind tunnel experiments and the MATLAB/Simulink control software to analyze the aerodynamic attributes of a tail fin-stabilized projectile with two different shapes and subsequently simulate its flight trajectory with four degrees of freedom under a flight condition 0.6 Mach. In the study comparing the CFD calculation results showed that the aerodynamic coefficients C_D , C_L , C_M , and C_{Ma} were similar within an angle of attack between $-8^\circ \sim 8^\circ$.

Lai et al. [30] discussed in their article, the effect of the wing-body combination on aerodynamic characteristics. The lift of the wing-body combination is not simply the addition of the lift of wing and lift of body alone, but the flow field across the whole wing-body has to be taken into consideration. The main objective of this project is to investigate the effect of fuselage diameter for both straight wing for high AR and low AR on the aerodynamic characteristics.

Ahmed et al. [31] presented in their study a six-degree-of-freedom nonlinear model, in the atmospheric flight, to predict the dynamic behavior of an advanced artillery projectile. The model is developed based on Newton's equations of motion. Furthermore, a modified standard atmospheric model to simulate air density and the speed of sound is

used. The aerodynamic forces and moments of the projectile body and lifting canards are a function of both Mach number and angle of attack. The analysis of the simulation results is discussed and shows that the impact accuracy of a conventional projectile using these course correction modules can be improved.

Tyler et al. [32] discussed in their thesis the design of an optimized nose shape of the projectile for minimum penetration of drag. This design is tested using the University of Alabama's supersonic wind tunnel and compared to shapes currently being utilized by the aerospace industry. A variety of analytical methods have been performed to optimize the nose shape for a penetrator. The results indicate that the newly defined nose with the least nose factor that would result in most penetration also results in the least aerodynamic drag over a Mach number ranges 1.85 to 3.1.

Besides the above-mentioned research, there had been unfathomable work and study on the aerodynamic characteristics of projectiles done by many researchers worldwide. Here I have highlighted only a few for the present study. In the above-mentioned research work, a study on aerodynamic characteristics was done only for a single type projectile. Here in this research, a study was done on the different types of projectiles.

CHAPTER-3

EXPERIMENTAL SET-UP

3.1 General

To study the aerodynamic characteristics of projectiles we need to use the variety of theoretical, experimental, and numerical methods. The experiment comprises the measurement of aerodynamic forces and moments on the model in the wind tunnel. The CFD simulation plays an important role in eliminating preliminary models at the beginning of the design process and leaving expensive wind tunnel testing for detailed models that are close to finding a design. The optimized design parameters is used for developing a numerical model and relationship between drag and lift coefficients with free stream velocity and angle of attack with the help of Ansys software.

3.2 Experiment

Presently, MIST has an open circuit subsonic wind tunnel in the fluid mechanics laboratory. This wind tunnel has a bell mouth entry, a flow Straightener, a diverging section, and two axial flow fans. The experiment was conducted in that wind tunnel where the hollow projectile individually and side by side was placed at the exit end of the wind tunnel. A set of hollow shape projectiles (37 mm, 57 mm, and a 125 mm) was considered for the experiment. The dimensions are collected from the commonly used shell in an anti-aircraft gun and also from a medium tank. At different angles of attack (less than 60°), the static pressure is measured. The speed of the wind tunnel (4.7 m/s) will be maintained at maximum to simulate the actual flow experienced by anti-aircraft gun projectiles. From the static pressure distributions, using numerical computations, the drag and lift coefficients will be measured and compared for a different size and flow configuration. For the numerical scheme, the ANSYS software will be used to simulate the experiment.

3.3 Preparation of Wooden Model

Projectiles of existing anti-aircraft Artillery and medium Tank of Bangladesh army were used for the preparation of the model. A solid works model of 57 mm projectile is shown in Figure 3. Here we have selected two anti-aircraft projectiles i.e. 57 mm & 37 mm and 125 mm projectile for medium Tank. We have prepared the dummy model by wood instead of metal because with the metal the dummy model will be heavier and will be difficult to use during the experiment. So each of the models was made of seasoned teak wood to avoid bucking and expansion due to the change in weather. Three wooden dummy model is shown in Figure 4. The diameter of the projectiles was 125 mm, 57 mm, and 37 mm shown in Figure 5. Each projectile contained 30 tapings for 125 mm projectiles and 17 & 10 for 57 & 37 mm projectile respectively. The distance between the consecutive tapping points was equal as shown in the Figure 6. Inner Diameter of each tapping point is 1 mm.

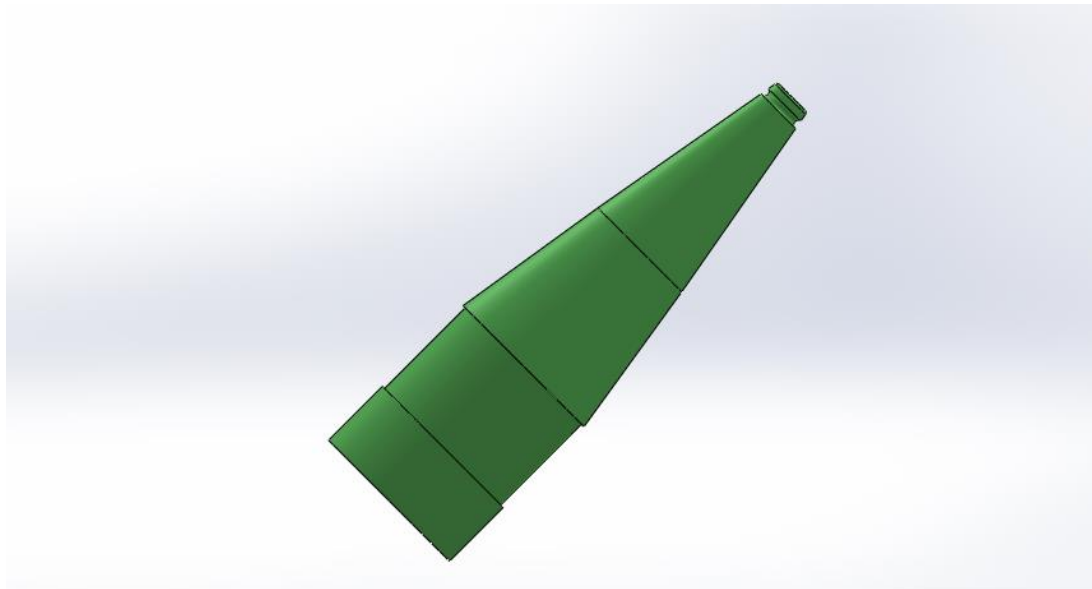


Figure 3: 3D model of the 57 mm projectile



Figure 4: Model Wooden Projectile of Different Size and Shape.

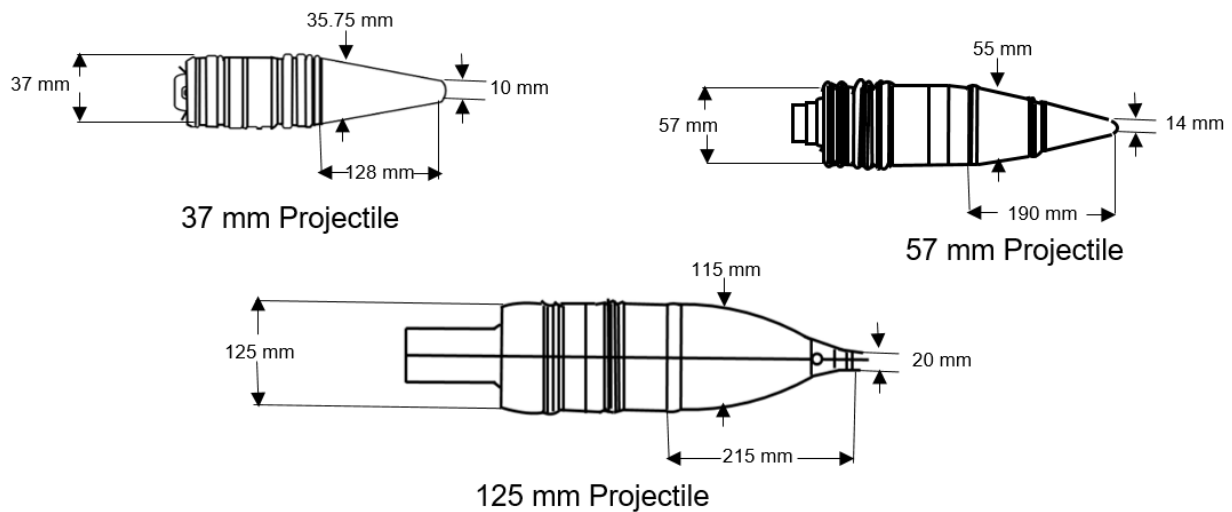


Figure 5: Various projectiles

Each tapping was identified by a numerical number from 1 to 30 for 125 mm projectile, 1 to 17 for 57 mm, and 1 to 10 for 37 mm projectiles. The tapping positions on the cross-section of the projectiles are shown in Figure 6. The tapings were made along the circular-section of the projectiles. Keeping the outside of the projectiles intact the inside of the projectiles was made hollow through which the plastic tubes were allowed to

pass. The plastic tubes were connected with the copper capillary tubes at one side and the other side with the inclined multi-manometer. The tapings were made of copper tubes of 2 mm outside diameter. Each tapping was of 50 mm length approximately. From the end of the copper tube flexible plastic tube of 1.5 mm, inner diameter was press-fitted.

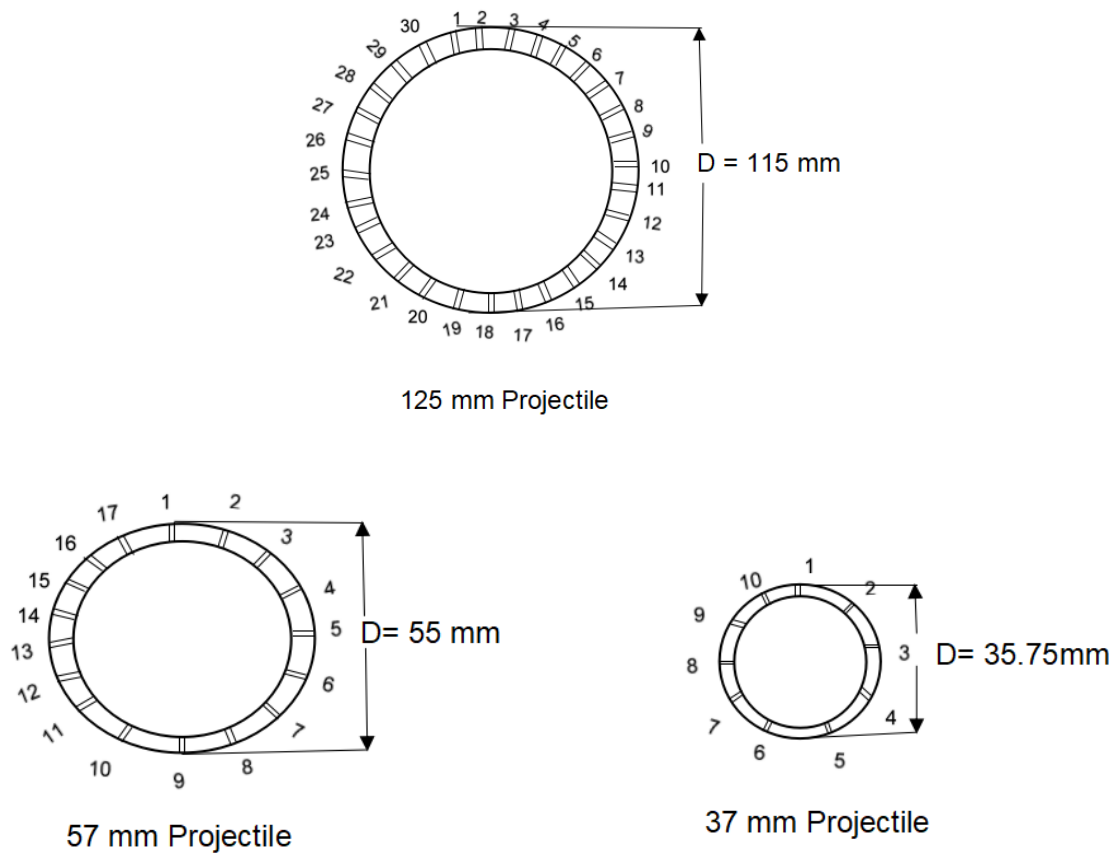


Figure 6: Tapping positions are shown on the cross-section of projectiles.

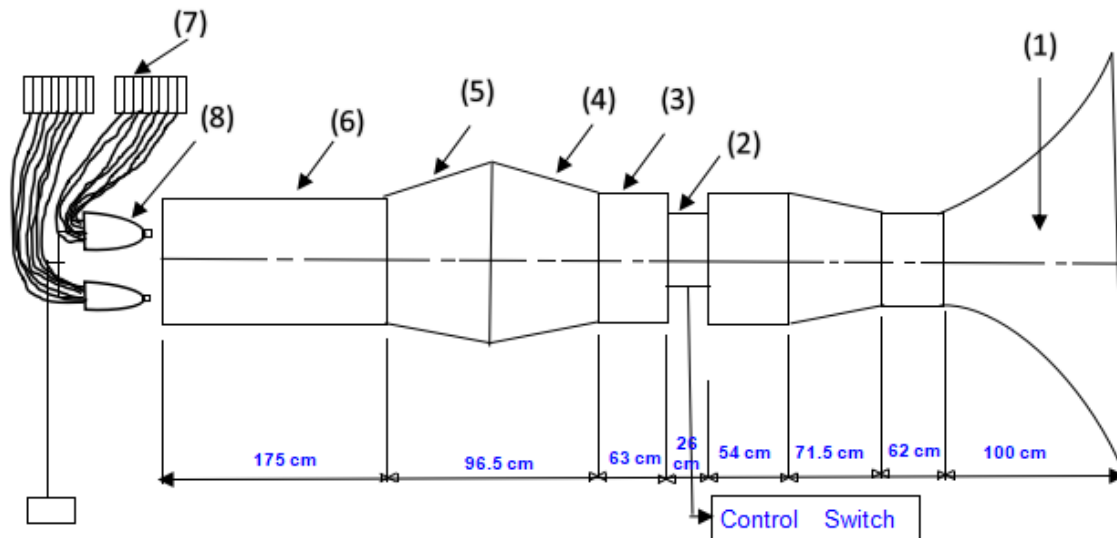
In the experimental investigation, one 125 mm, one 57 mm, and one 37 mm projectiles were used. The initial reading was taken placing the single projectile in front of the wind tunnel shown in Figure 7.



Figure 7: Experimental setup of 57 mm projectile for measuring static pressure.

3.4 Wind Tunnel

The test was done in an open circuit subsonic wind tunnel as shown in Figure 8. It was the low-speed wind tunnel having the maximum wind velocity of 4.7 m/s in the test section. The tunnel consists of various components such as fan, valve, silencer, honeycomb flow straightener. It is 6.16-meter-long with a test section of 490-mm x 490-mm cross-section. To make the flow uniform a honeycomb is fixed near the end of the wind tunnel. There is a converging bell mouth shaped entry. To generate the wind velocity, two axial flow fans are used.



- | | | |
|---------------|-----------------------|-----------------------|
| 1. Inlet duct | 4. Diverging section | 7. Inclined Manometer |
| 2. Fan | 5. Converging section | 8. Dummy projectile |
| 3. Silencer | 6. Flow straightener | |

Figure 8: Schematic diagram of a wind tunnel

Each of the fans is connected with the motor of 2.25 kilowatt and 2900 rpm. There is a regulator to control the wind speed. There is a silencer as shown in the figure. The control longitudinal axis of the wind tunnel is maintained at a constant height of 1010 mm from the floor. The axis of the model coincides with that of the wind tunnel. The converging mouth entry is incorporated in the wind tunnel for smooth entry of air into the tunnel and to maintain uniform flow into the duct-free from outside disturbances. The induced flow through the wind tunnel is produced by a one-stage rotating axial flow fan of capacity 10.20 m³/s at the head of 152.4 mm of water and 1475 rpm.

A variable frequency drive is used to control the flow. A silencer is fitted at the end of the flow controlling section to reduce the noise of the system. This section is incorporated with a honeycomb. The diverging and converging section of the wind tunnel

is 965 mm long and made of 18 GMS sheets. The angle of divergence and convergence is 29° which has been done to minimize expansion and contraction loss and reduce the possibility of flow separation. After the diverging section, there is a 175 cm long flow straightener to convert the angular flow into straight & horizontal directions. Wind velocity is measured directly with the help of a digital anemometer. The flow velocity in the test section is 4.7 m/s approximately.

3.5 Test Section

The reading was taken at the exit end of the wind tunnel in the open air as shown in Figure 8. The projectiles were placed with a stand at the same level as the wind tunnel at the exit end. In the middle of the hollow cylinder, it was made groove and connected with a plastic tube. Either side of the plastic tube is connected with an inclined multi-manometer. Each circular projectile was equally spaced and made a total of 30 grooves for 125 mm projectiles, 16 grooves for 57 mm, and 10 grooves for 37 mm anti-aircraft artillery projectile. Each manometer is made with 30 tubes and connected with projectile grooves. 30 scales were fixed along the 30 tubes in the manometer to take the reading.

Since the top and bottom of the extended part of the wind tunnel was open; as such no correction for the blockage was done in the analysis. The projectiles were placed very close to the exit end of the wind tunnel so that the approach velocity of a projectile was approximately identical as that in the exit end of the wind tunnel. The projectiles were placed at the exit end of the wind tunnel first line at 30° angle of elevation. Then it was gradually elevated at the interval of 5° each and data is recorded. In this way, projectiles were elevated up to 50° and necessary data was recorded and subsequently, calculations are carried out.

3.6 Measuring Equipment

The wind velocity across the test section of the wind tunnel was measured with the help of a digital anemometer. A pitot tube was also used to measure the velocity to cross-check. The pitot tube was connected to an inclined manometer and the limb of which contained manometer fluid. The surface static pressures were measured with the help of an inclined manometer. The inclination of the manometer was sufficient to record the pressure with reasonable accuracy.

3.7 Experimental Conditions

There were three projectiles and the number of tapping points around the projectiles was different for all three projectiles. The static pressure was measured with a manometer and it had a minimum deflection of 1 mm. The experimental conditions are shown in Table 1. A Computational Fluid Dynamics (CFD) simulation was done with ANSYS Multiphysics software on similar conditions to compare the experimental and simulation results.

Table 1. Experimental Conditions for Different Projectiles.

Projectile Size (mm)	The angle of Attack, AOA, (°)	Air Velocity (m/s)	Number of Tapping Points	Reynolds no Re
37	30, 35, 40, 45, 50	4.7	10	11,770
57	30, 35, 40, 45, 50	4.7	17	18,131
125	30, 35, 40, 45, 50	4.7	30	39,762

CHAPTER- 4

MATHEMATICAL MODEL AND SIMULATION

4.1 Mathematical Model

In this chapter, from the wind tunnel pressure tap, static pressure at the upstream of the test section was measured for calculating the lift and drag force. The inclined manometer was used to measure the static pressure on the projectile surface. A constant Wind Velocity of the Wind tunnel was chosen which was 4.7 m /s, measured directly with an anemometer which is later used to calculate the drag, lift, and pressure coefficient.

The wooden projectiles were prepared with the help of the original dummy projectiles shown in Figure 9. The projectiles were made with seasoned teak wood to avoid any kind of shape deformation. A lathe machine was used to make the projectile and holes are made to insert a small tube to measure static pressure on the projectile surface.



Figure 9. Wooden Projectiles Manufactured.

4.2 Determination of Pressure Coefficient

The pressure coefficient is a dimensionless number which describes the relative pressures throughout a flow field in fluid dynamics. The pressure is measured at the tapping by using Equation 1.

$$P = \Delta l_k \rho_k g \dots\dots\dots(1)$$

Where

P = Static Pressure

Δl_k = Manometer reading

ρ_k = Density of Kerosene

g = Gravitational Acceleration

Now the pressure coefficient can be determine from the following equation:

$$C_p = \frac{\Delta P}{0.5 * \rho_{air} U_{\infty}^2}$$

Where, $\Delta P = P - P_{\infty}$

P = Static pressure on the surface of the projectile

P_{∞} = The ambient pressure

ρ_{air} = the density of the air

U_{∞} = the free stream velocity

In our experiment ΔP can be obtained from the manometer reading.

4.3 Determination of Drag and Lift Coefficient

Drag coefficient is a dimensionless quantity that is used to quantify the drag or resistance of an object. The drag coefficient (C_D) is defined as

$$C_D = \frac{2 * L_D}{S_{Total} * \rho_k * U_{\infty}^2}$$

Where:

L_D = is the drag force.

ρ_k = is the mass density of the fluid,

U_{∞} = is the flow speed of the object relative to the fluid,

S_{Total} = is the reference area

Here the acting force on a single segment (assuming segment 1) is calculated from Equation 2.

$$F_1 = P * S_{Projected 1} \dots \dots \dots (2)$$

Then the Total Force acting on the Projectile will be

$$F = F_1 + F_2 + F_3 + \dots \dots \dots + F_n \dots \dots \dots (3)$$

As the air is coming at an angle, therefore, the Total forces will be divided into Horizontal and Vertical direction. If the Angle of Attack is ' α ' then the drag and lift force is calculated from Equation 4 and 5.

$$L_D = F \cos \alpha \dots \dots \dots (4)$$

$$L_L = F \sin \alpha \dots \dots \dots (5)$$

Now with the help of Drag and Lift forces, Drag and Lift Coefficient can be determined.

Lift coefficient is a dimensionless coefficient that relates the lift generated by a lifting body. The lift coefficient is defined (C_L) by

$$C_L = \frac{2 * L_L}{S_{Total} * \rho_k * U_{\infty}^2}$$

Where,

S_{Total} = Total Active Projected Area ($S_1+S_2+S_3+\dots+S_n$)

A SolidWorks model for each projectile is made and the projected area of each strip is measured by using SolidWorks 'evaluate' tool. The segment numbers on the projectiles are different. The top and bottom surface of the projectile is segmented into equal segments and they are connected with 3D drawings. A 2D drawing was drawn on a plane facing the air and the area of all segments was not calculated. The back of the projectile can not be seen due to the angle as they can not be seen from the front of the plane facing the wind, turbulence could create fluctuating pressure in those manometer reading and not very dependable. Figures 10, 11, and 12 show the projected area measurement by SolidWorks.

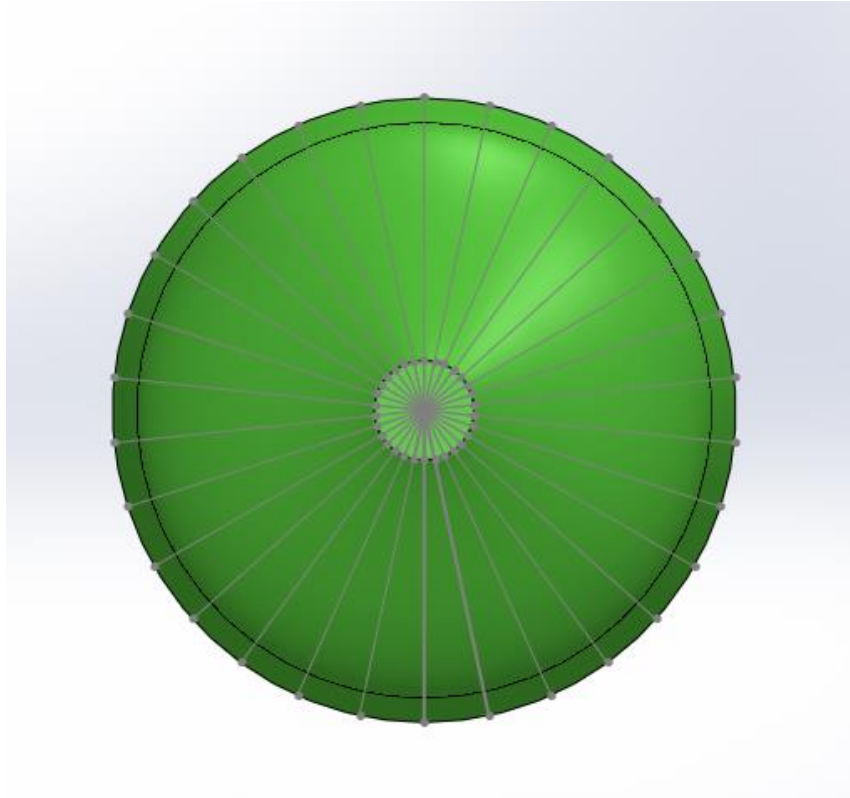


Figure 10: Plane view of the Projectile form air direction

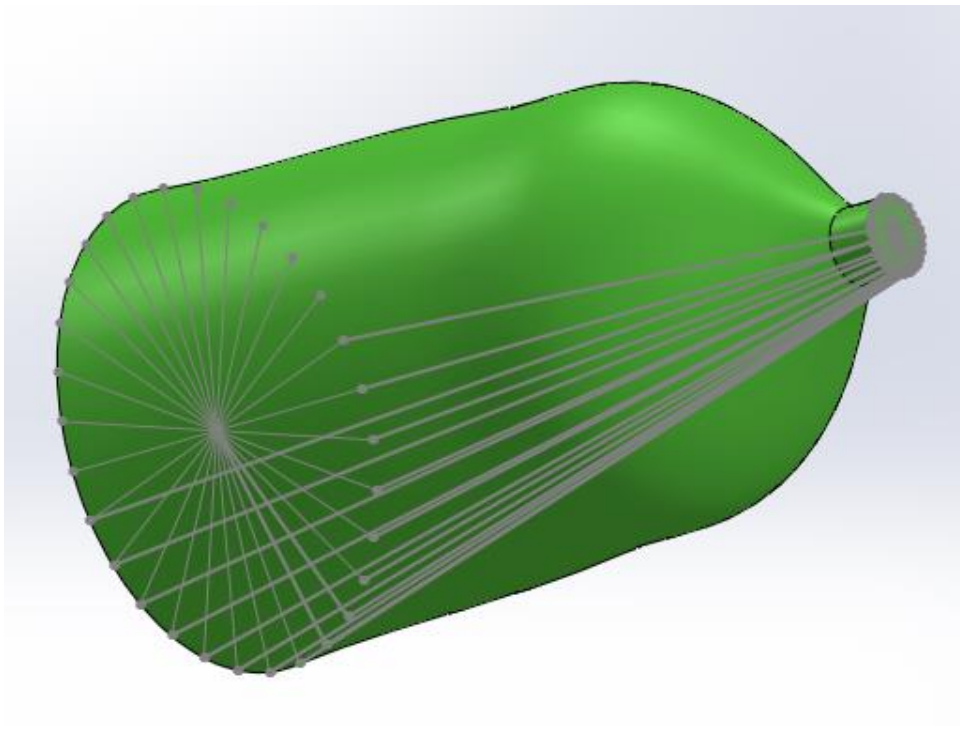


Figure 11: Area has drawn from the projection of the segments.

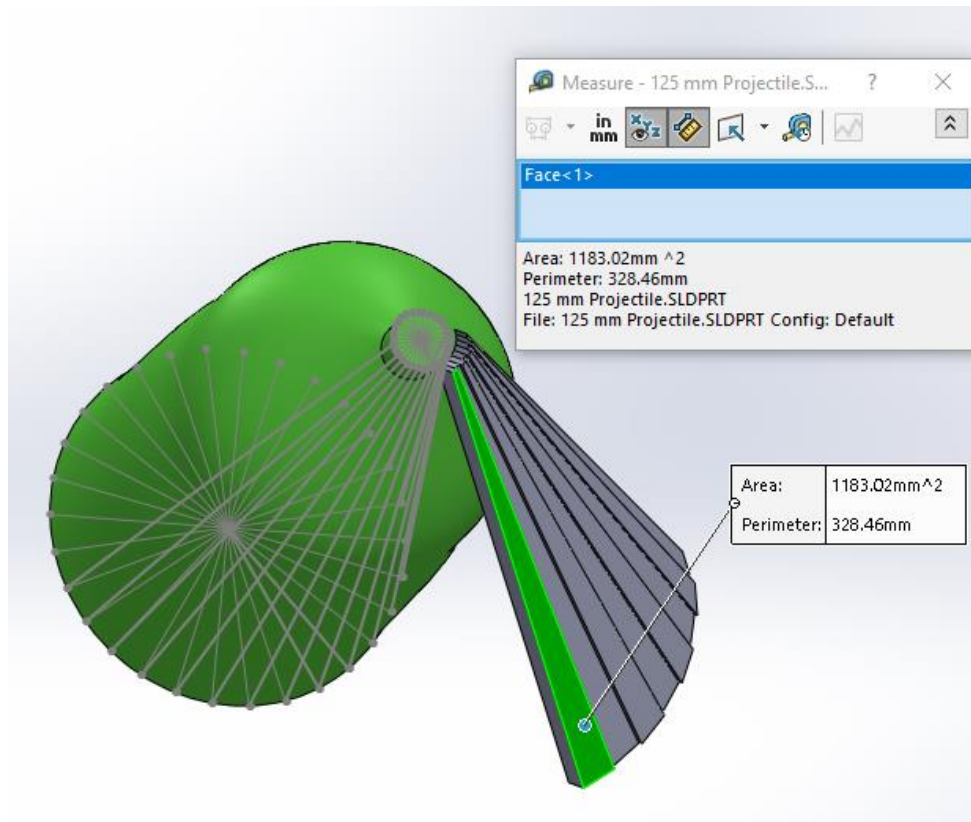
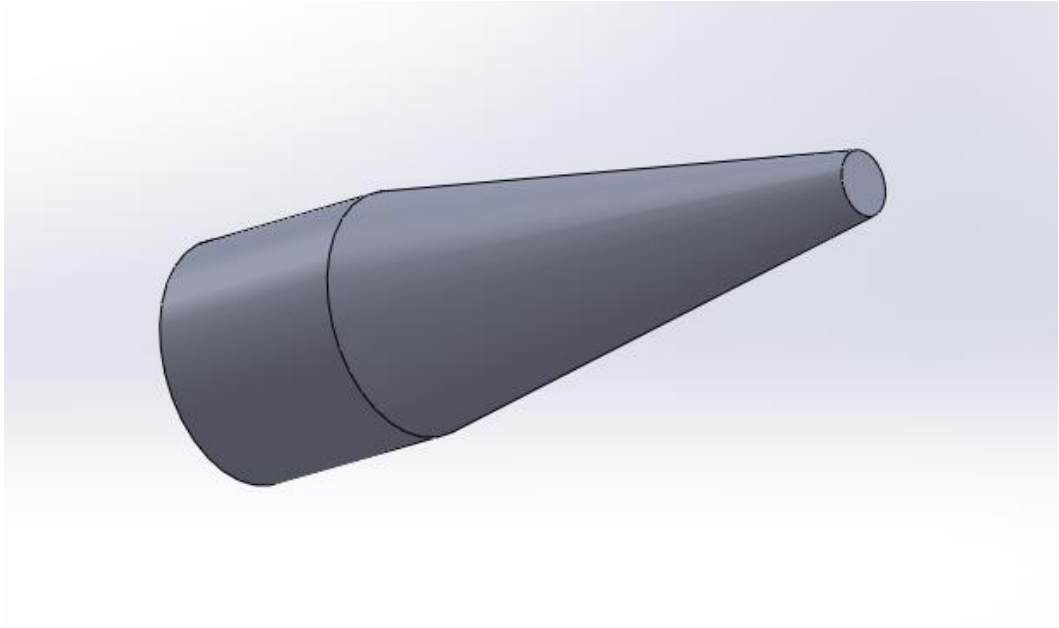


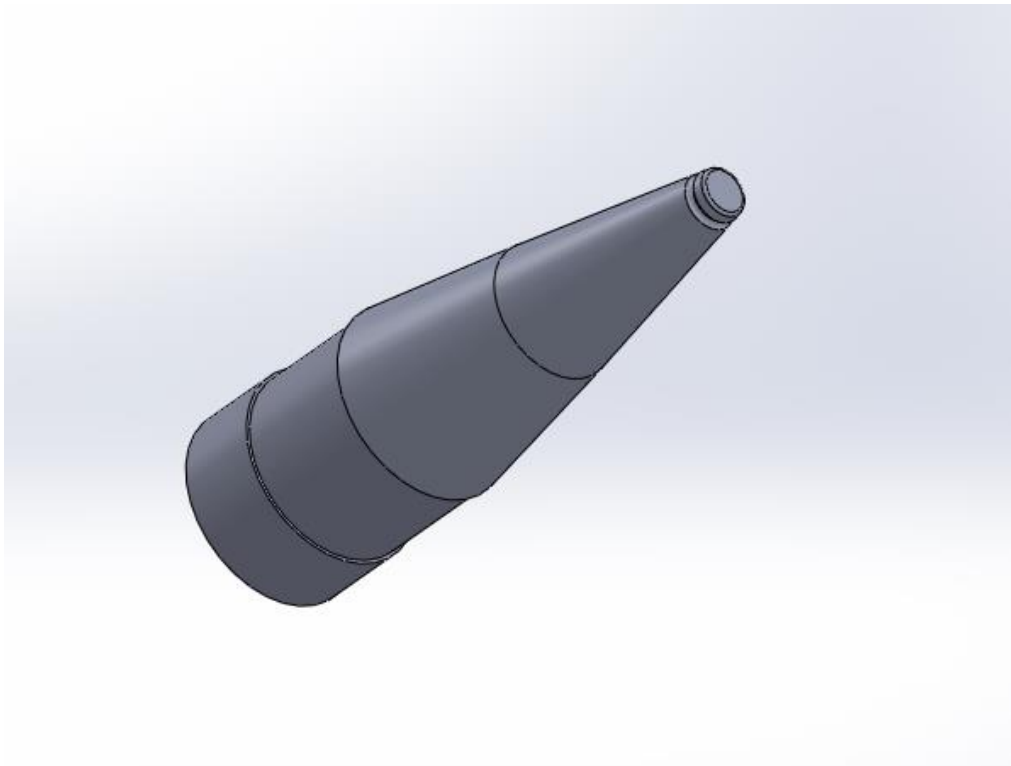
Figure 12: Measurement of the projected area.

4.4 Geometrical setup

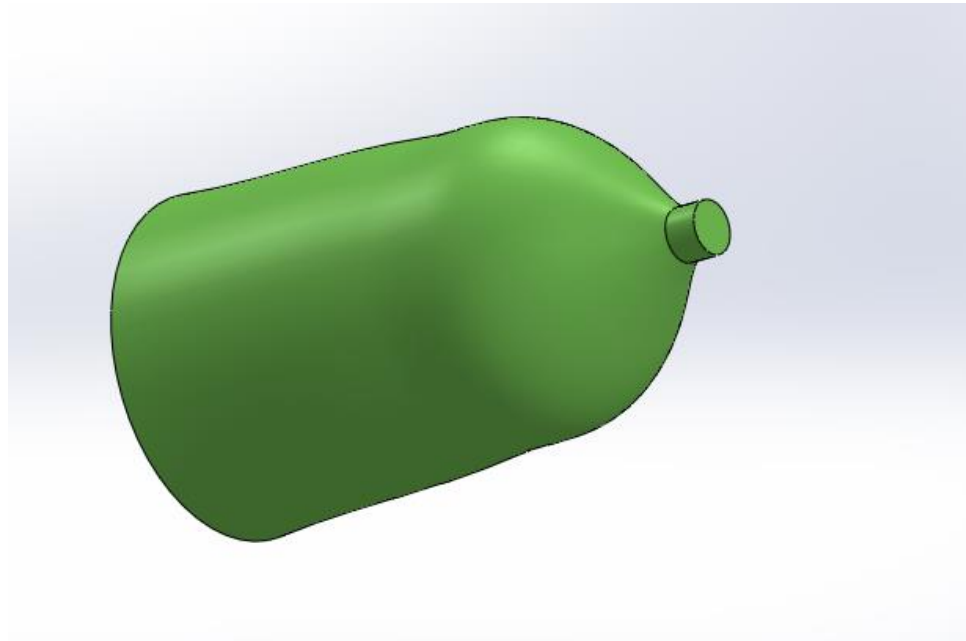
For the computational simulation, we need to prepare the geometry of the projectile. Here we have considered the dimensions of 37 mm, 57 mm, and 125 mm projectiles. With the help of solid works, we have developed the geometry of the projectile. The Solid Works model was made for measuring the projected area which is used for simulation. Ansys software is used to analyze the CFD model. Numerical results are highly influenced by the dimensions of the geometrical domain. The projectile is considered as a solid domain and outside of it is considered as air domain. The $k-\epsilon$ turbulence model is used for solving the problem. The inlet condition was 4.7 m/s air and outlet condition was atmospheric condition similar to experiment. The rest of the surface is considered a wall. Figure 13 (a), (b), (c) shows the geometry of the 37, 57, and 125 mm projectiles.



(a)



(b)



(c)

Figure 13. Geometry files for CFD simulation (a) 37 mm, (b)57 mm, and (c) 125 mm Projectiles.

4.5 Simulation and Mesh Settings

An unstructured meshing of the projectile was done for rendering a computer screen and for physical simulation i.e for finite element analysis or CFD. It is a subdivision of a continuous geometric space into a discrete geometric cell. Here resolution of the meshing was greater in the regions where greater computational accuracy was needed. It is done at 45° having the boundary condition greater than the projectile. The mesh file for simulation is shown in Figure 14 and the simulation settings for the projectiles are shown in Figure 15.

The geometry of the projectiles with the same dimension of was put forward to simulation with scale 1:1. The geometric model of the projectile is shown in Fig. No 13. The projectile model was sketched on Solid Works 2017 then imported to ANSYS

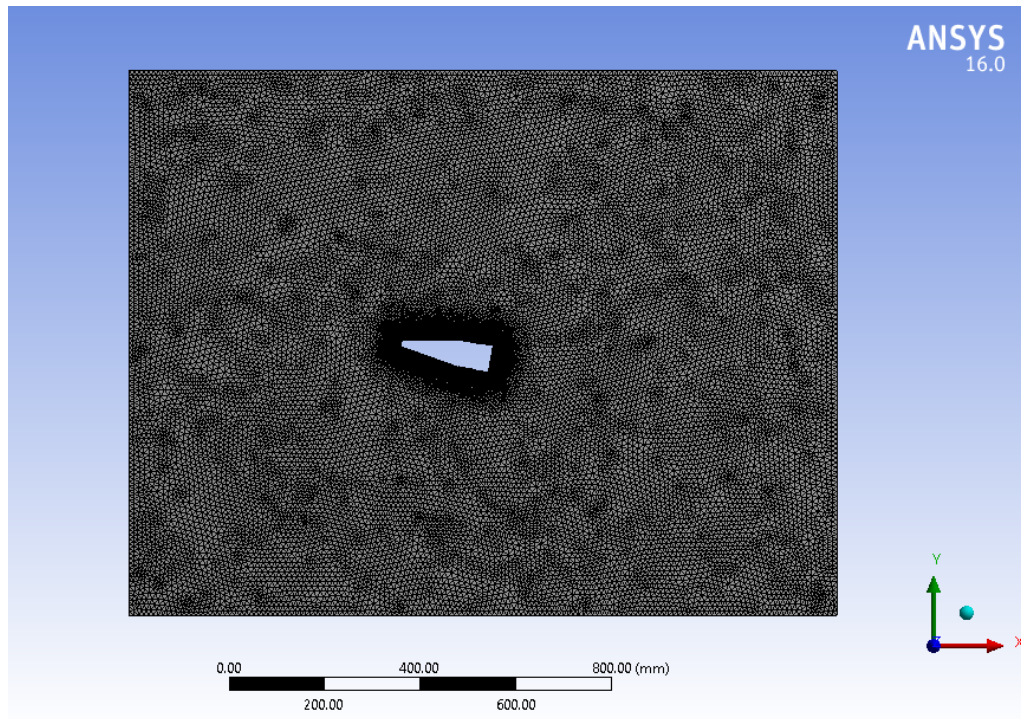
Geometry. The boundary is C-type pattern with 10D at the upstream side and 15D at the downstream side from the surface of the model where D is the diameter of the projectile.

In the problem, the platform of pre-processing ICEM, CFD 16.0, the unstructured grid (An unstructured mesh is defined as a set of elements, commonly tetrahedrons, with an explicitly defined connectivity. The unstructured mesh generation process involves two basic steps: point creation and definition of connectivity between these points. Flexibility and automation make the unstructured mesh a favorable choice. Some other advantages of unstructured grid over structured are save time and fast convergence rate.) was adopted, after that inflation layer was employed to densify gird around the model to improve numerical precision. The number of the nodes in the mesh generated is 3619040 elements, 4891536 nodes. The results obtained during the grid dependency tests a finer mesh, made of 3619040 elements, 4891536 numbers of nodes are compared with a coarse mesh of 167932 elements and 183564 numbers of nodes. The pressure coefficient found for the finer mesh varies with the coarse mesh by 0.64% which is concurrent to the independency test. The grid Independency test table is shown in Table 2.

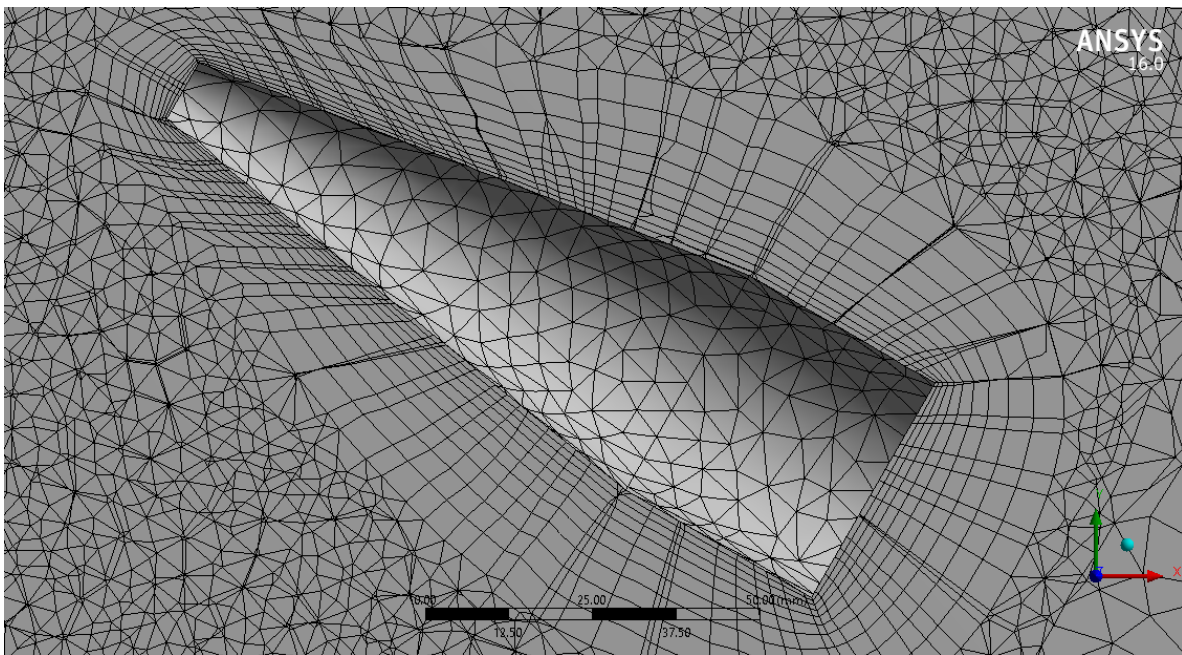
Table 2. Grid Independency Test

Nodes	Elements	C_d	Error(%)
183564	167932	1.514573	-
236870	196743	1.099573	37.74
345230	278345	0.891262	23.37
567723	498726	0.774565	15.07
908357	698216	0.713574	8.55
1453370	977502	0.674476	5.80
2325393	1368504	0.659037	2.34
3720629	1915905	0.649753	1.43
4173893	2682268	0.645354	0.68
4891536	3619040	0.641274	0.64

The air enters into the domain with a velocity of 4.7 m/s. The density of air was 1.225 kg/m³ and viscosity about 1.7894e-05 kg/m-s. At the outlet, the pressure outlet condition is applied in the domain. The steady and incompressible flow of air is considered in this Analysis. The solution procedure adopted to solve the CFD model using FVM solver. The default solver settings are selected because a pressure based solver is used to solve the steady-state problem. Atmospheric pressure is maintained at outlet and Ansys uses the default value (0 Pa for gauge pressure). In these calculations, the second-order upwind scheme based on a multidimensional linear reconstruction approach is used. The SIMPLE algorithm for pressure velocity coupling with a second-order upwind discretization scheme is used to obtain a solution for the equations of Momentum, Turbulence Kinetic Energy, and Turbulence Dissipation Rate. The target of all discretization techniques in FVM is to develop a mathematical model to convert each of the terms into an algebraic equation. Once implemented to complete control volumes in a particular mesh, we attain a full linear system of equations that requires to be solved. These computations are carried out using FVM solver (ANSYS FLUENT 2016), a commercial CFD package with a 3D double-precision Configuration. The default convergence criterion in FLUENT is maintained. This criterion requires that the scaled residuals decrease to 10⁻⁵. Ansys CFD Simulation shown in figure: 16.

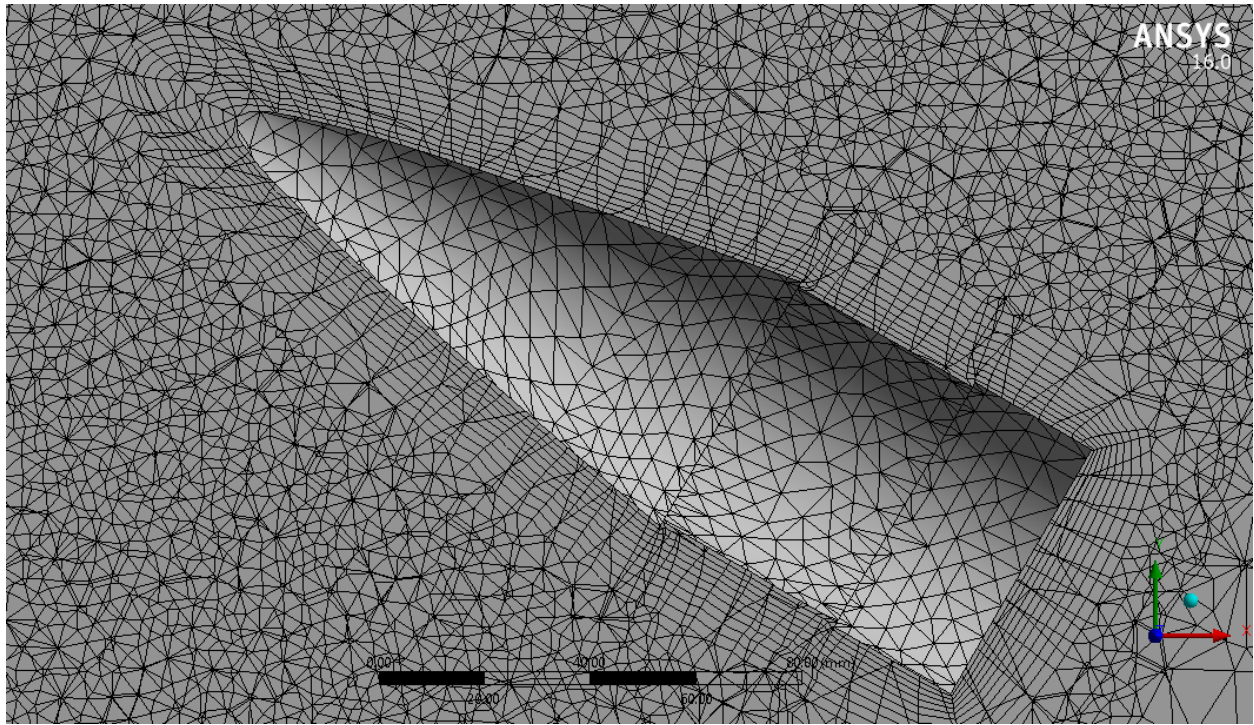


(a)

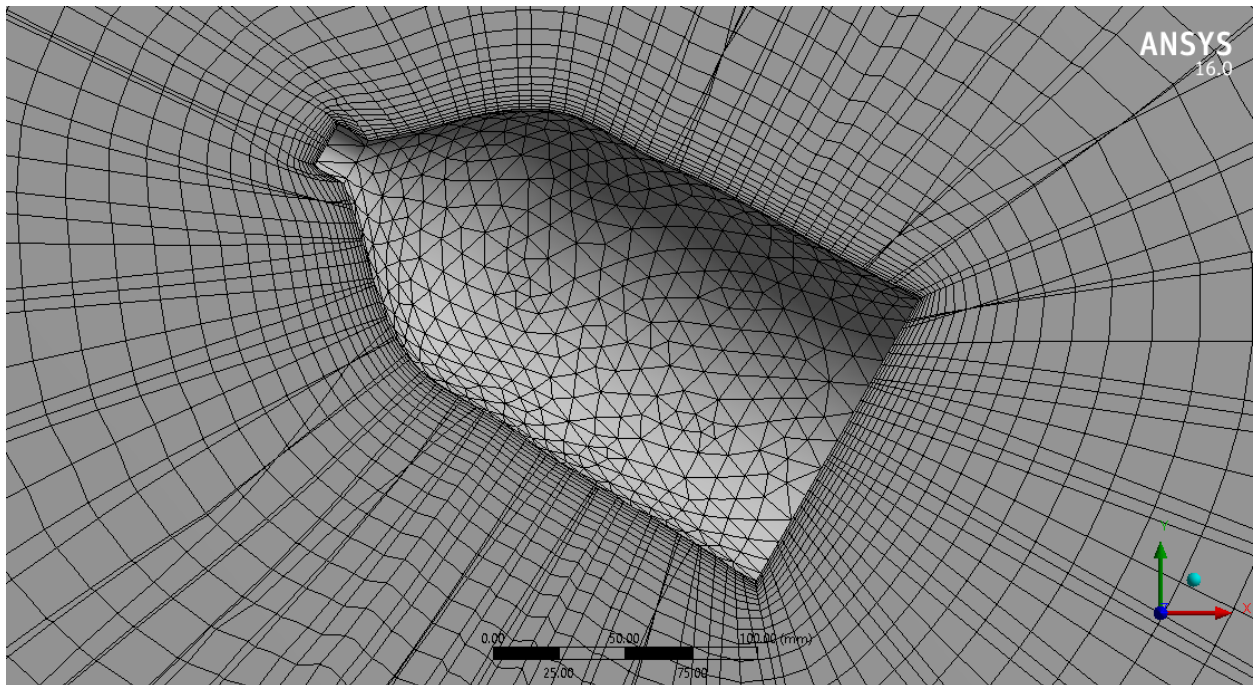


(b)

Figure 14. Mesh of the CFD Simulation for (a) 37 mm, (b) 37 mm (zoomed) Projectiles.

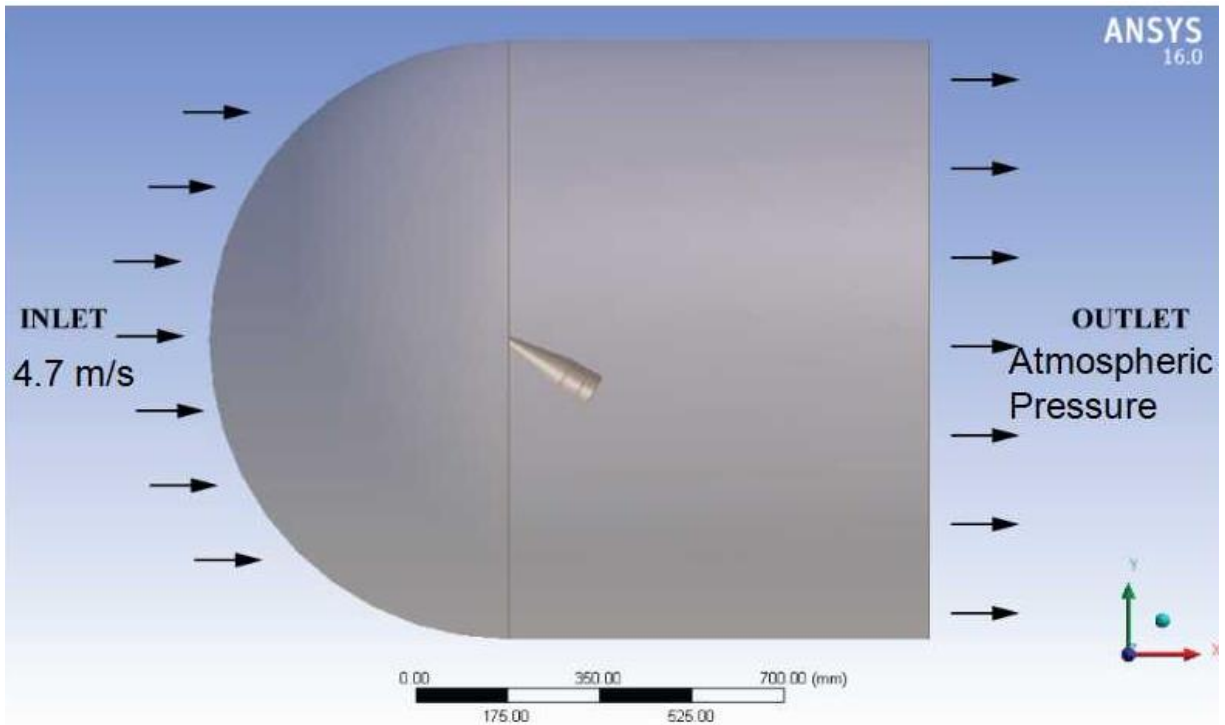


(a)

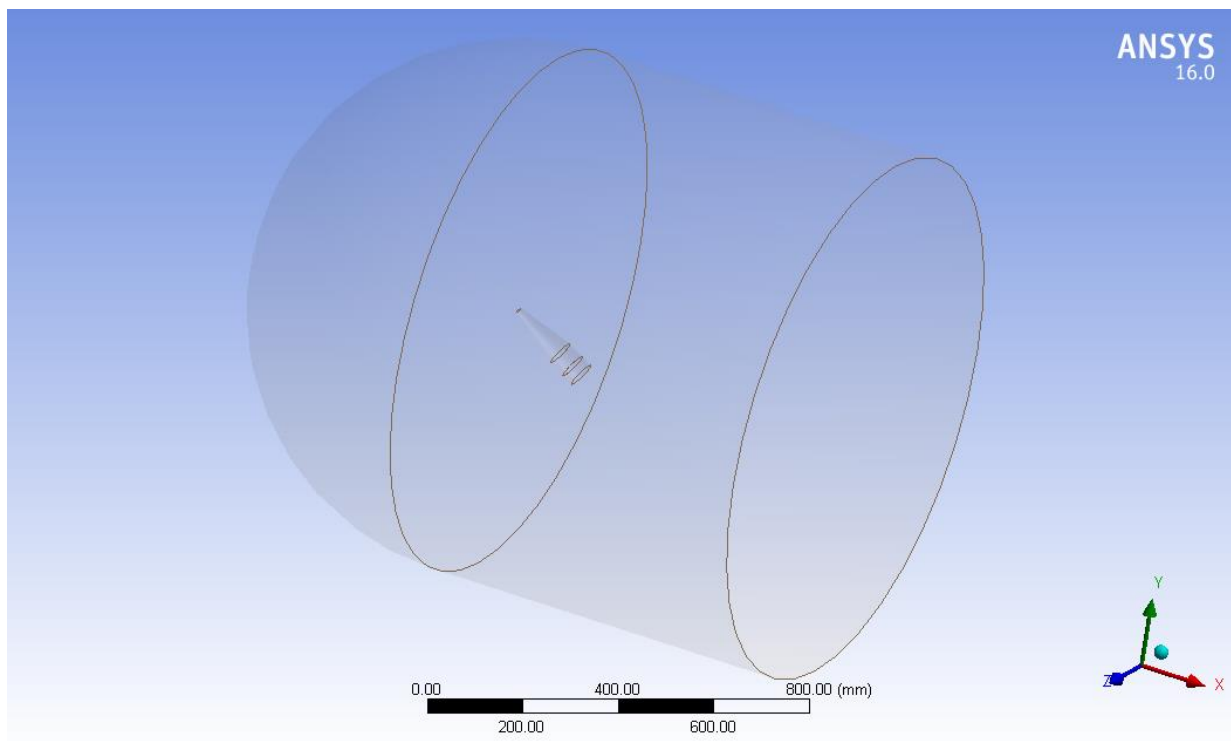


(b)

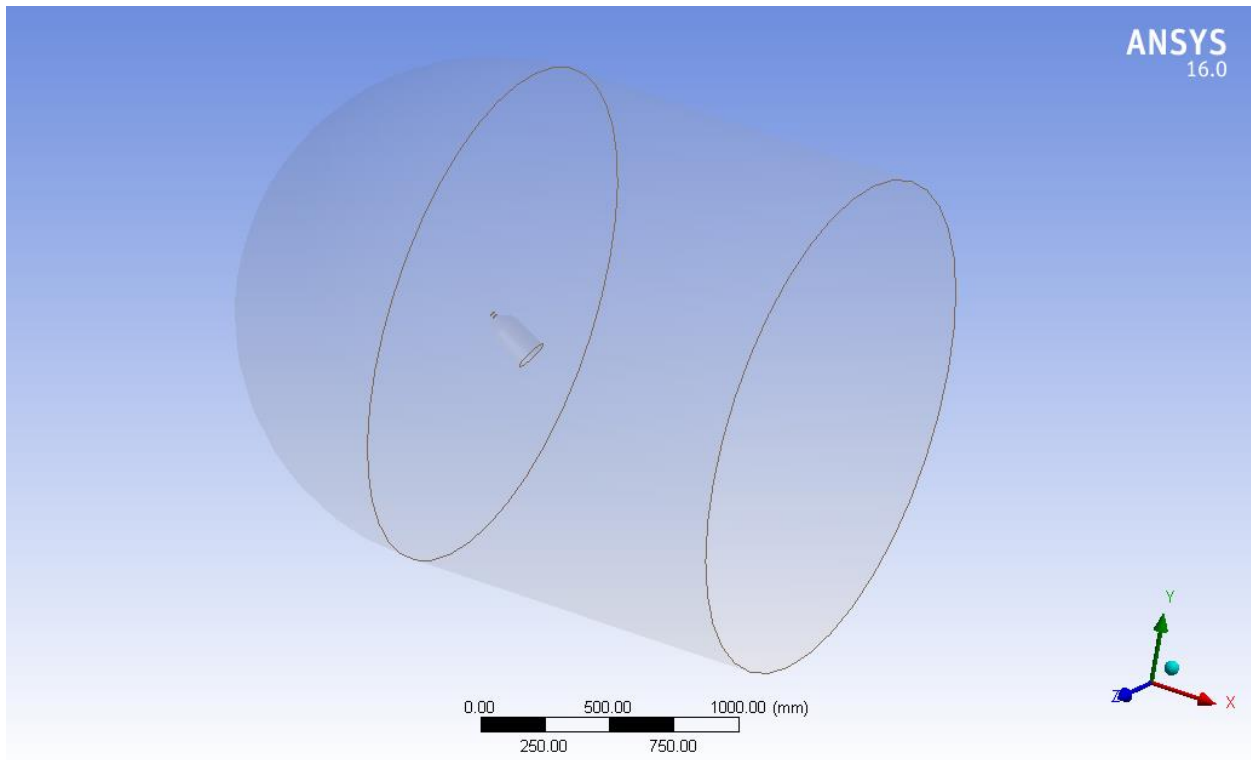
Figure 15. Mesh of the CFD Simulation for (a) 57 mm, and (b) 125 mm Projectiles.



(a)



(b)



(c)

Figure 16: Ansys CFD Simulation setting for (a) 37mm, (b) 57 mm, and (c) 125 mm Projectiles.

CHAPTER- 5

RESULTS AND DISCUSSION

5.1 General

Here the results of the experimental and numerical investigation regarding the surface static pressure coefficients, drag and lift coefficients are discussed. Initially, the static pressure on the surface of the projectiles at various angles of attack was taken into consideration. Then the distribution of the static pressure coefficients on the surface of the projectile is compared with the numerical study. The calculated drag and lift coefficients for the group of projectiles are also compared in the same way.

There are some assumptions made, such as, room temperature and humidity is considered as constant. In reality the density of the air changes due to the temperature and humidity. Another such assumption was the density of the manometer fluid and theoretical value was considered for the calculations.

Due to the turbulence at the backside of the projectile, the manometer reading was observed fluctuating. But that fluctuation was not significant as measuring the projected area from the AOA was impossible. While taking the reading, always the mean value of the manometer was recorded hence incorporate some inaccuracy. The scale beside the manometer has a precision of 1.0 mm deflection. Therefore, it was quite difficult to measure the deflection of the manometer fluid column below 1 mm. This measurement error reflects in the calculations and plot and the conclusion that we have drawn.

5.2 Discussion of the Results

The projectiles are not only different in sizes they are also unique in their shapes. Therefore, the possibility of drag forces and lift forces could be different as the drag force and Lift forces are a function of the shapes. The static pressure acting on the projectiles are calculated from the manometer reading, projected area, and the angle of attack. The friction of the projectile is not considered in the simulated evaluation. But the surface friction has a contribution to the drag force and lift forces. Some manometer showed positive and some manometer showed negative deflection (the passing air is creating suction i.e. vacuum). The total force acting on the projectile can be determined by combining the drag and lift forces acting on each segment of the projectiles. For the same angle of attack such as at 50° , the drag forces for 37, 57, and 125 mm projectile are 0.0224 N, 0.0492 N, and 0.1629N. The lift forces also increase from 0.0159 N to 0.0382 N, and 0.1296 N for 37, 57, and 125 mm projectiles.

The drag and lift forces found to be the function of the angle of attack as well. As the angle of attack increases the drag and lift forces increases as well. The drag forces are almost constant if the angle of attack is low. The lift forces increase for aerofoil shape with the angle of attack and the pilot of an aircraft rotate the nose of the aircraft just before the take-off to increase the angle of attack. In this investigation, the rate of increasing the lift forces is more than the drag forces. It was found that the drag force increasing rate is 54.4% for 57 mm projectile and 86.2% for 125 mm projectile. The lift force increasing rate is 58% for 57 mm projectile and 87.87% for 125 mm projectile. Therefore, a large size projectile may have large drag but due to large surface area and angle of attack, the lift force increases as well.

There were at least 3 sets of data measured for each experimental conditions. The average value was taken for calculation so the uncertainty of the measured data is

removed. Moreover, the increasing rate of drag and lift coefficients were taken from the least square fitted plot and comparing by their differences in the slope. The higher the slope the higher is the rate for that particular set of data.

There was some deviation between the experimental and simulated findings which can be coming from the lack of precision measurement, the ignored friction coefficient of the projectile surface, and the geometrical inaccuracy due to manual fabrication. The increase in the drag and lift forces are common for all the projectiles. Figure 17 and 18 shows the drag and lift forces at different attack angle. The corresponding data sets are shown in Tables 3 and 4.

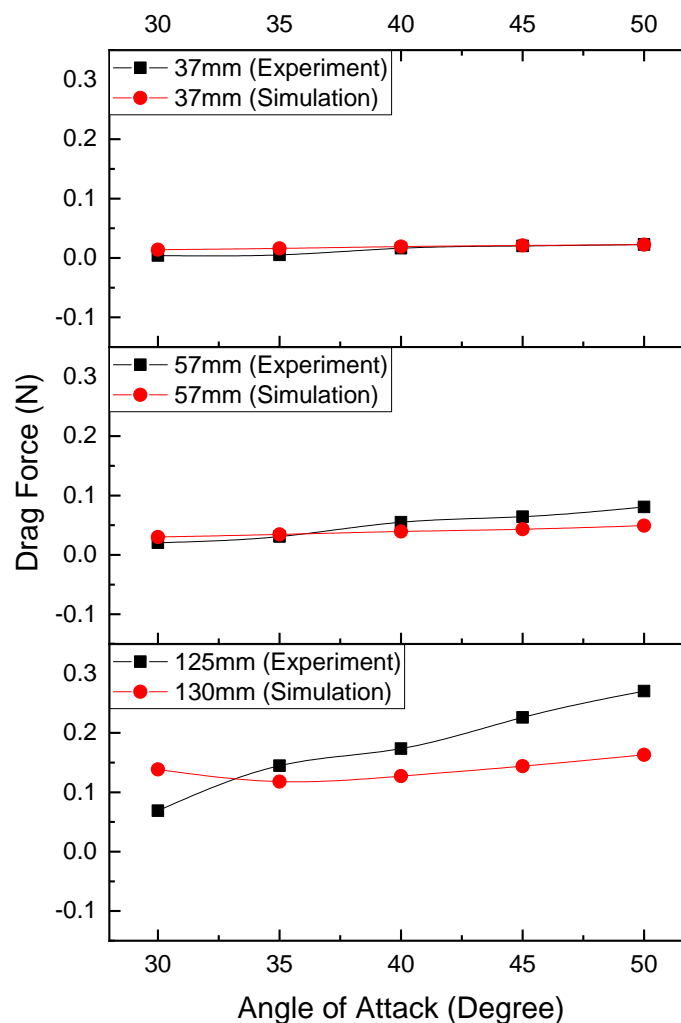


Figure 17: Angle of Attack Vs Drag Force.

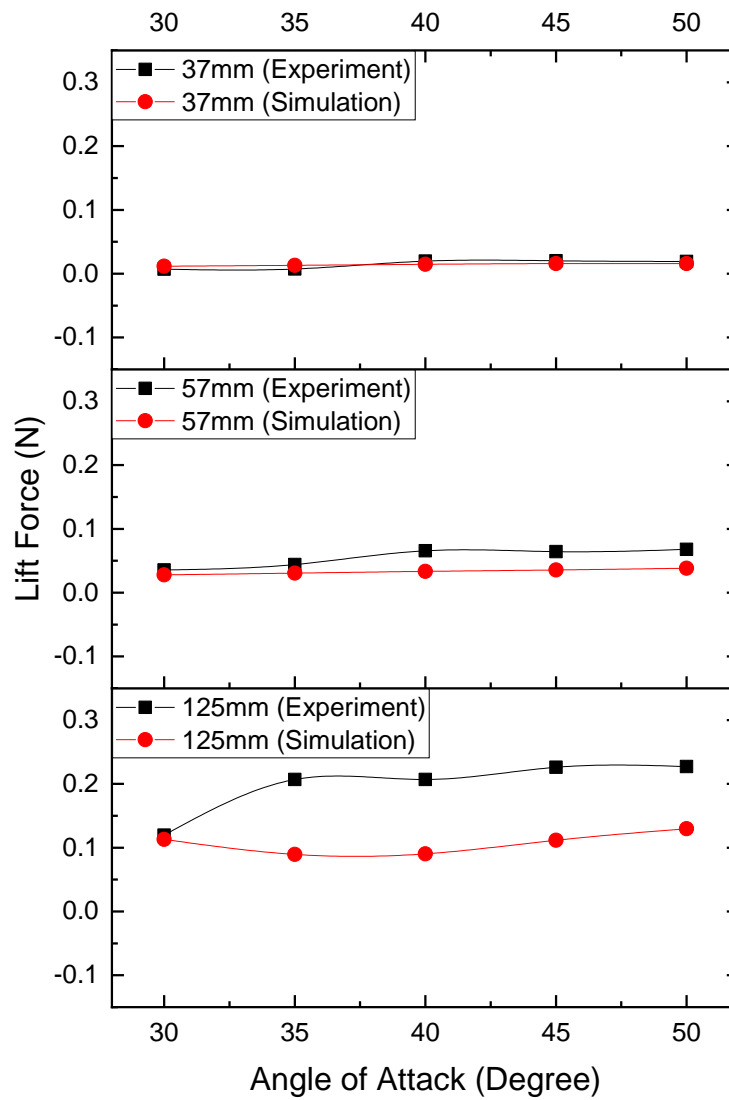


Figure 18 : Angle of Attack vs Lift Force.

Table 3: Simulation and Experimental Drag Forces on 37, 57, and 125 mm Projectiles at Different AOA.

Angle of Attack (°)	37S (N)	57S (N)	125S (N)	37E (N)	57E (N)	125E (N)
30	0.0138	0.0300	0.1384	0.0040	0.0204	0.0689
35	0.0162	0.0345	0.1180	0.0051	0.0308	0.1447
40	0.0192	0.0393	0.1272	0.0164	0.0551	0.1735
45	0.0211	0.0431	0.1439	0.0201	0.0643	0.2259
50	0.0224	0.0492	0.1629	0.0227	0.0806	0.2704

Table 4: Simulation and Experimental Lift Forces on 37, 57, and 125 mm Projectiles at Different AOA

Angle of Attack (°)	37S (N)	57S (N)	125S (N)	37E (N)	57E (N)	125E (N)
30	0.0116	0.0278	0.1131	0.00696	0.0355	0.1195
35	0.0132	0.0306	0.0895	0.00741	0.0441	0.2068
40	0.0146	0.0332	0.0904	0.01959	0.0657	0.2069
45	0.0159	0.0355	0.1116	0.0201	0.0644	0.2261
50	0.0159	0.0382	0.1296	0.0190	0.0677	0.2271

The simulated and experimental drag and lift coefficients are plotted in Figures 19 and 20. The overall experimental drag coefficients are higher than simulated drag coefficients except for 37 mm projectile where the experimental drag coefficients slightly lower than the simulation. The deviation between the experimental and simulated results may be the result of measurement inaccuracies, geometrical inaccuracies, and ignored surface roughness. The projectiles are made with a manual lathe and therefore, the manufacturing deviation could play a vital role in the deviation of the results.

A very similar observation was found by Alexey et al. [37] where until the airspeed reaches 1.1-1.2 Mach number the drag coefficient increases and then started to reduce. Hemateza et al [38] have found from the simulation that, the Drag Coefficient has increased as the AOA increased which is found in our case. The test airspeed in the subsonic zone is the major limitation in our experiment. Performing the test in the

supersonic wind tunnel will enable us to investigate the parameters in more detail. Table 5 and Table 6 shows the corresponding data for drag and lift coefficients.

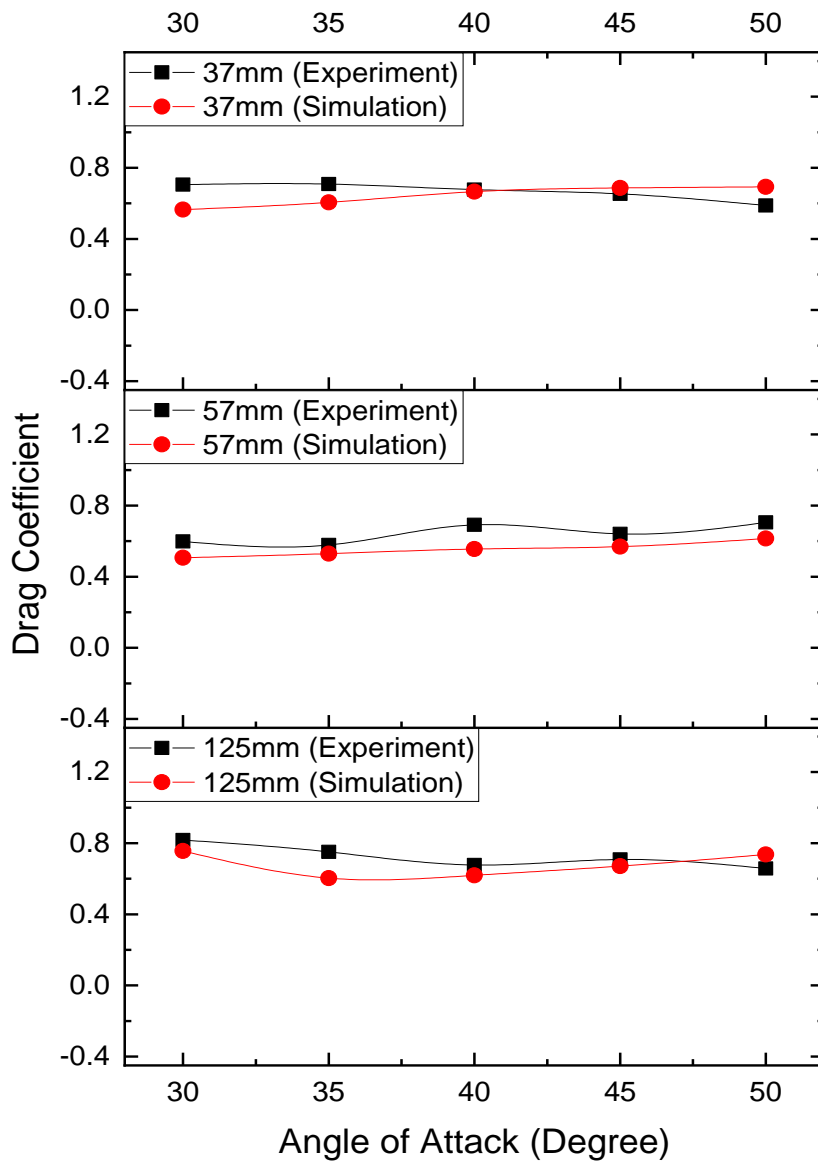


Figure 19 : Angle of Attack vs Drag Coefficients.

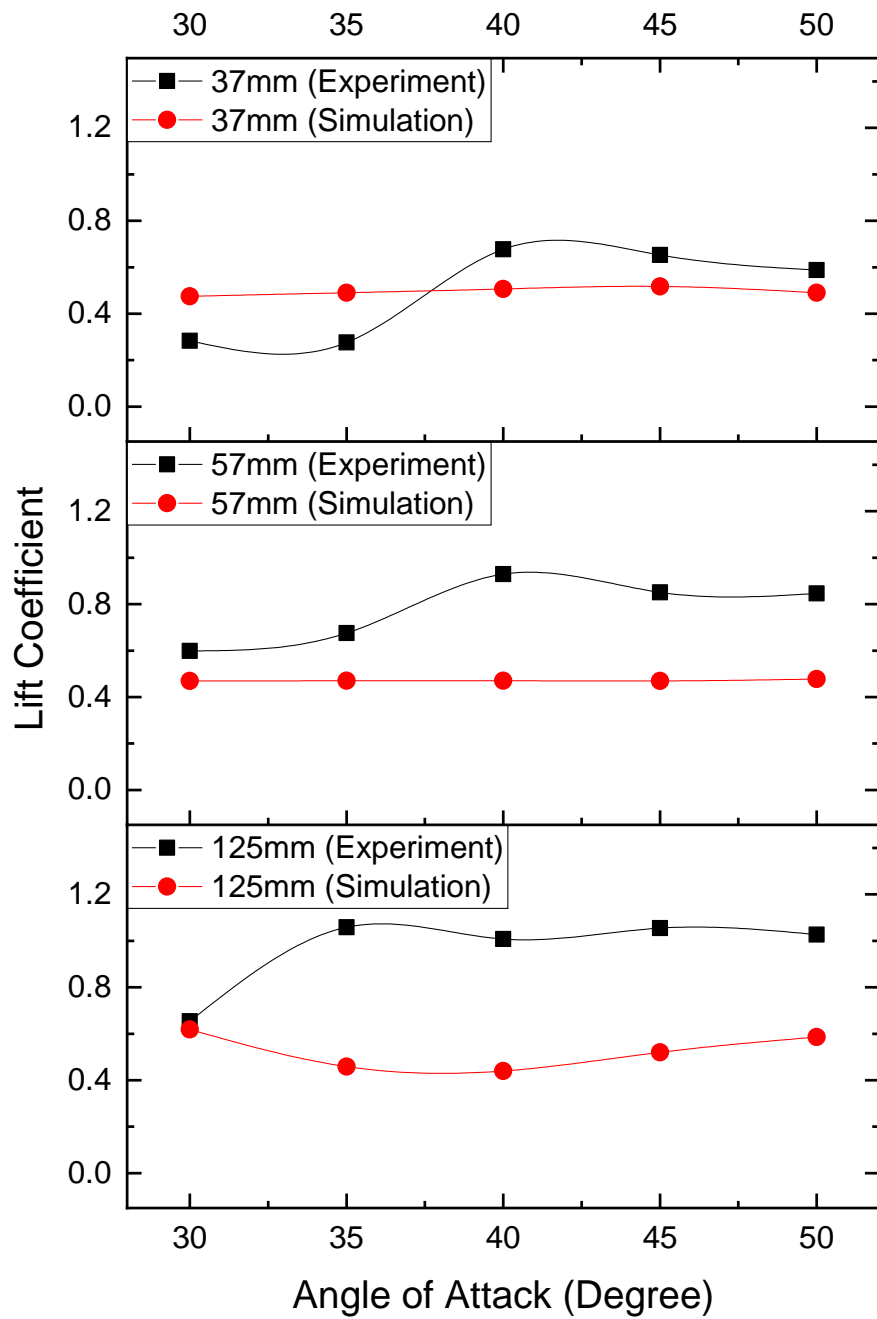


Figure 20: Angle of Attack vs Lift Coefficients.

Table 5: Simulation and Experimental Drag Coefficients on 37, 57, and 125 mm Projectiles at Different AOA

Angle of Attack (°)	37S	57S	125S	37E	57E	125E	37 S-E Error(%)	57 S-E Error(%)	125 S-E Error(%)
30	0.0158	0.033	0.138	0.0173	0.036	0.149	8.4	6.8	7.49
35	0.0162	0.035	0.118	0.0190	0.038	0.147	14.5	8.3	19.5
40	0.0193	0.044	0.127	0.0196	0.049	0.139	1.76	9.5	8.5
45	0.0211	0.043	0.144	0.0201	0.049	0.152	5.08	11.1	5.2
50	0.0225	0.049	0.163	0.0191	0.056	0.145	17.7	12.8	12.0

Table 6: Simulation and Experimental Lift Coefficients on 37, 57, and 125 mm Projectiles at Different AOA

Angle of Attack (°)	37S	57S	125S	37E	57E	125E	37 S-E Error(%)	57 S-E Error(%)	125 S-E Error(%)
30	0.012	0.023	0.083	0.009	0.020	0.086	16.6	11.6	3.7
35	0.013	0.031	0.089	0.013	0.026	0.103	1.0	16.2	12.7
40	0.015	0.035	0.109	0.016	0.041	0.117	10.8	14.1	6.4
45	0.019	0.046	0.131	0.020	0.048	0.152	5.7	6.1	13.3
50	0.02	0.058	0.149	0.023	0.067	0.173	12.3	13.3	13.5

The pressure coefficient is calculated and plotted against the tapping points on the projectiles. The pressure coefficients at the tapping points that are facing the air gradually decreasing and increasing. The measurement at the back of the projectile is very fluctuating as turbulence was observed in the back. Therefore, the pressure coefficients at the back of the projectile are not dependable. It was also observed that the turbulence felt at the back of the projectile is related to the size of the projectile. The turbulence decreased as the projectile size increased from 37 mm to 57 mm shown in Figure 21, Figure 22, and Figure 23.

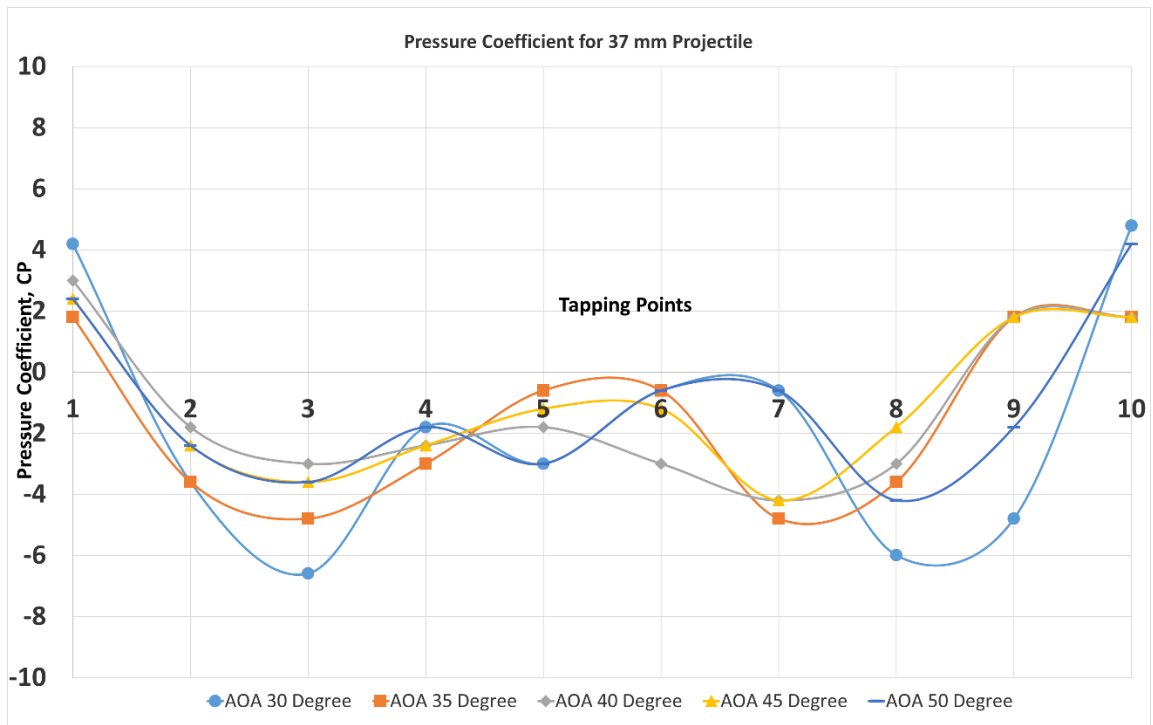


Figure 21 : Tapping Point Vs Pressure Coefficients for 37 mm Projectile.

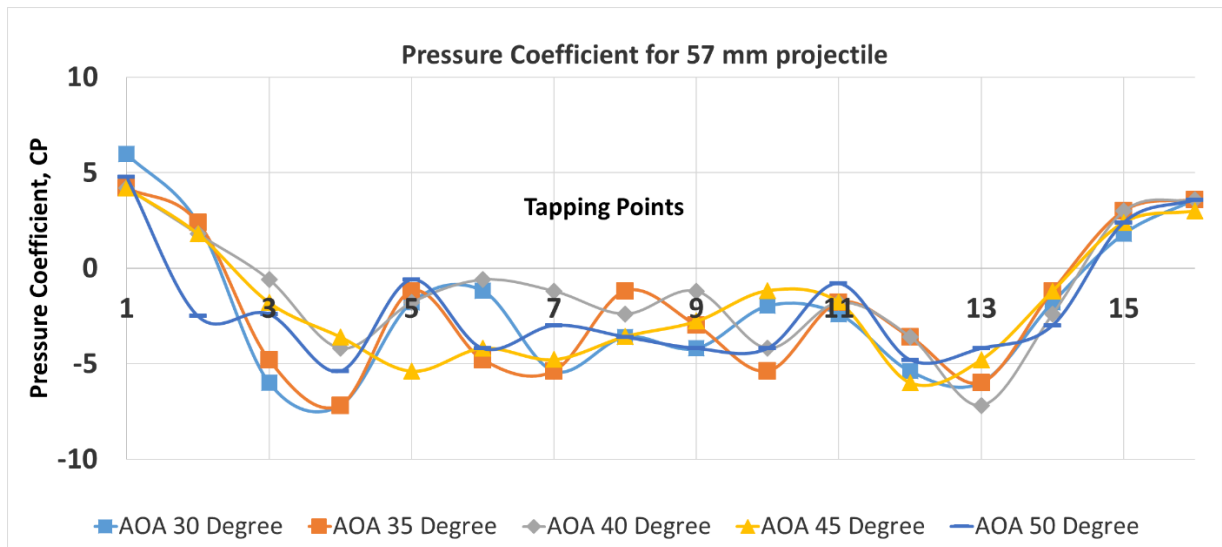


Figure 22 : Tapping Point Vs Pressure Coefficients for 57 mm Projectile.

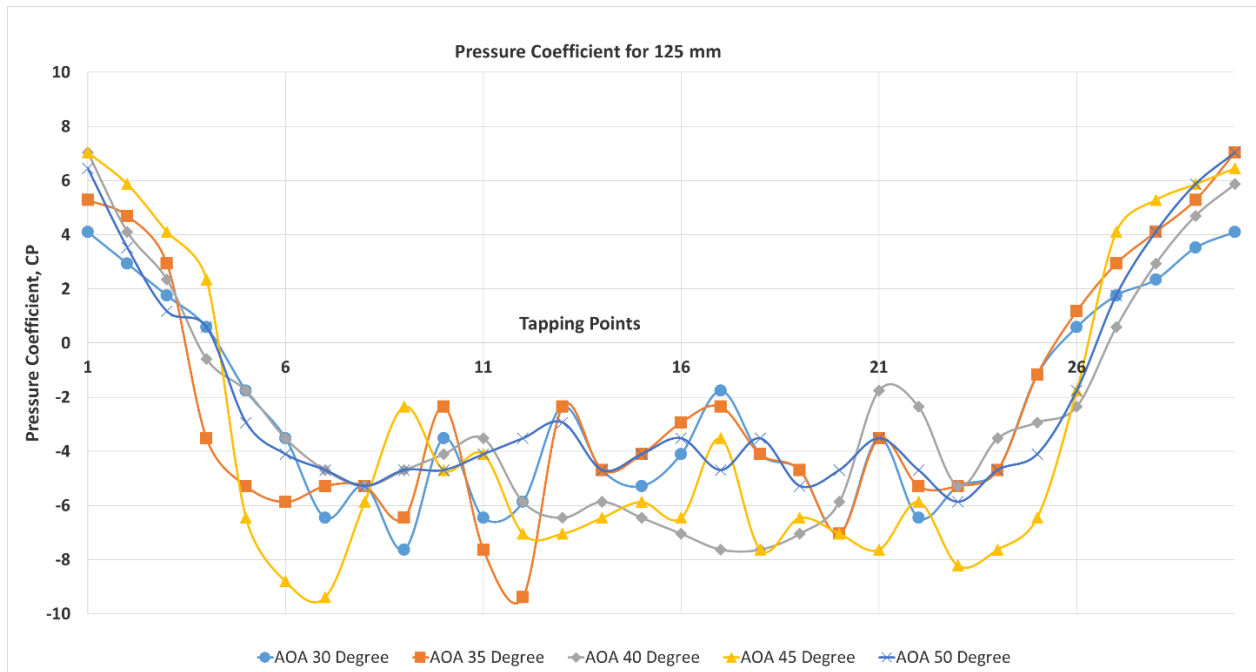


Figure 23: Tapping Point Vs Pressure Coefficients for 125 mm Projectile.

5.3 Pressure and Velocity Simulation

The simulation pressure and velocity plots are shown for 37 mm, 57 mm, and 125 mm projectiles in Figures 24, 25, 26, 27, 28 and 29. The velocity plot shows the turbulence due to the shape of the projectiles. As the projectile size increases, the visual streamline from the simulation shows that the smaller size projectile gets more turbulence compared to the large size projectile. The velocity of the air increases as the streamline passes over the projectile. The reason could be the shape of the projectiles.

The pressure was mostly felt at the front of the projectile at 45° angle regardless of their sizes and shapes. However, the velocity streamline plots show that the streamline is flowing over the 37 mm projectile. The 57 mm and 125 mm projectile does not show any streamline flowing over them. Therefore, the drag forces should be higher for larger projectiles.

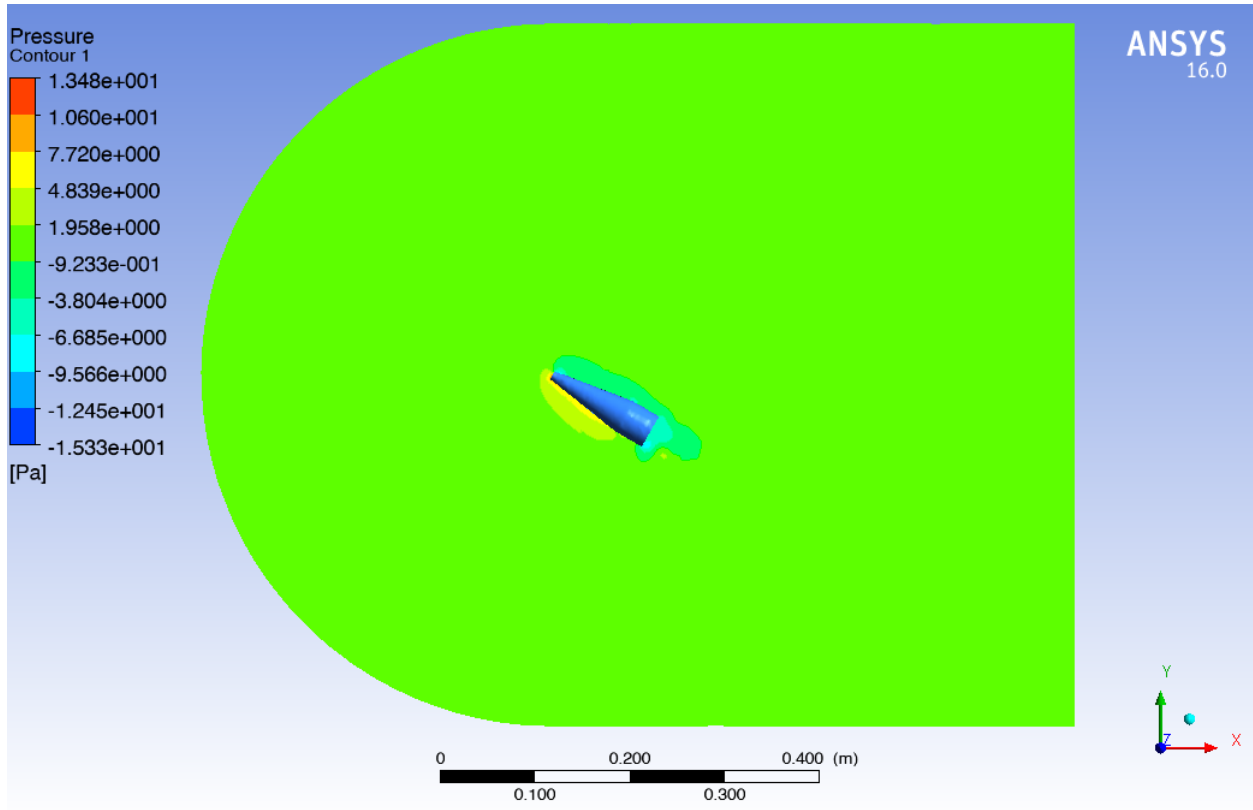


Figure 24 : The pressure contour for 37 mm projectile at 45°AOA.

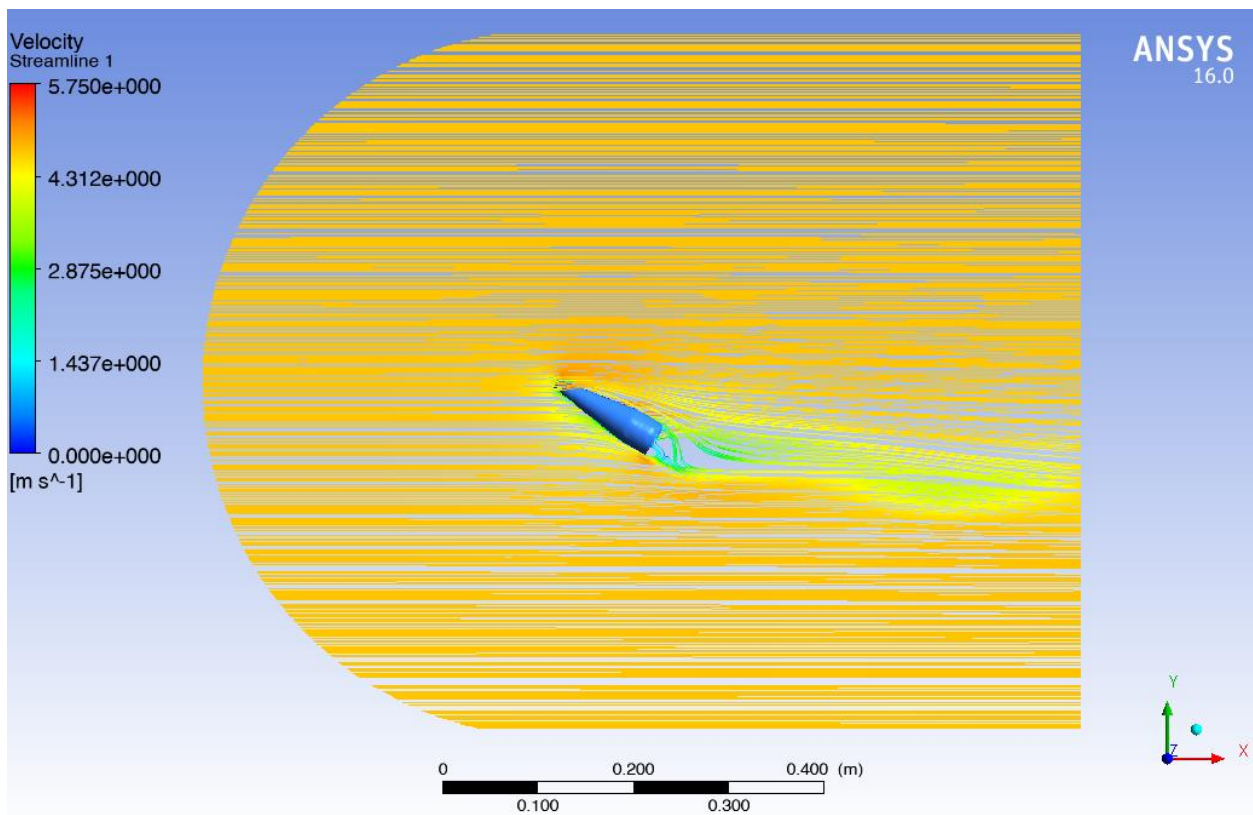


Figure 25 : The velocity contour for 37 mm projectile at 45°AOA.

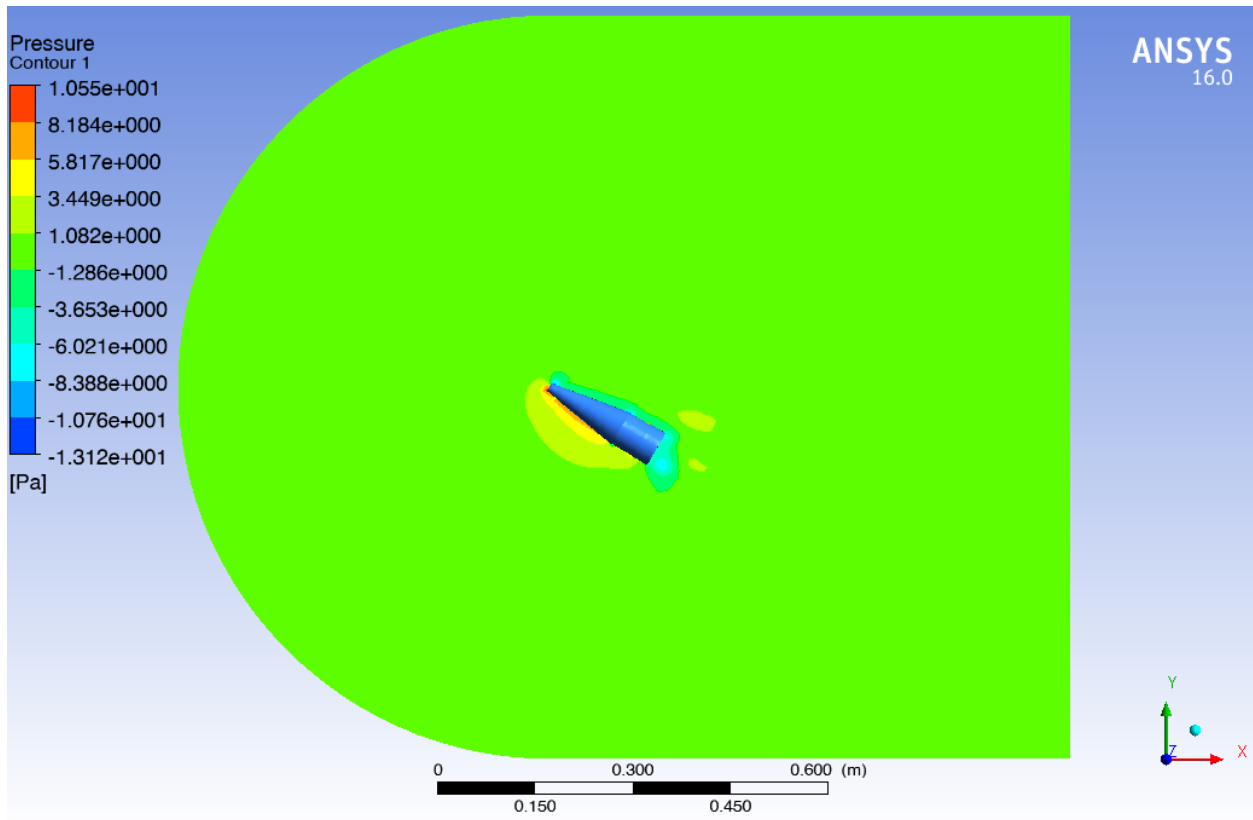


Figure 26 : The pressure contour for 57 mm projectile at 45° AOA.

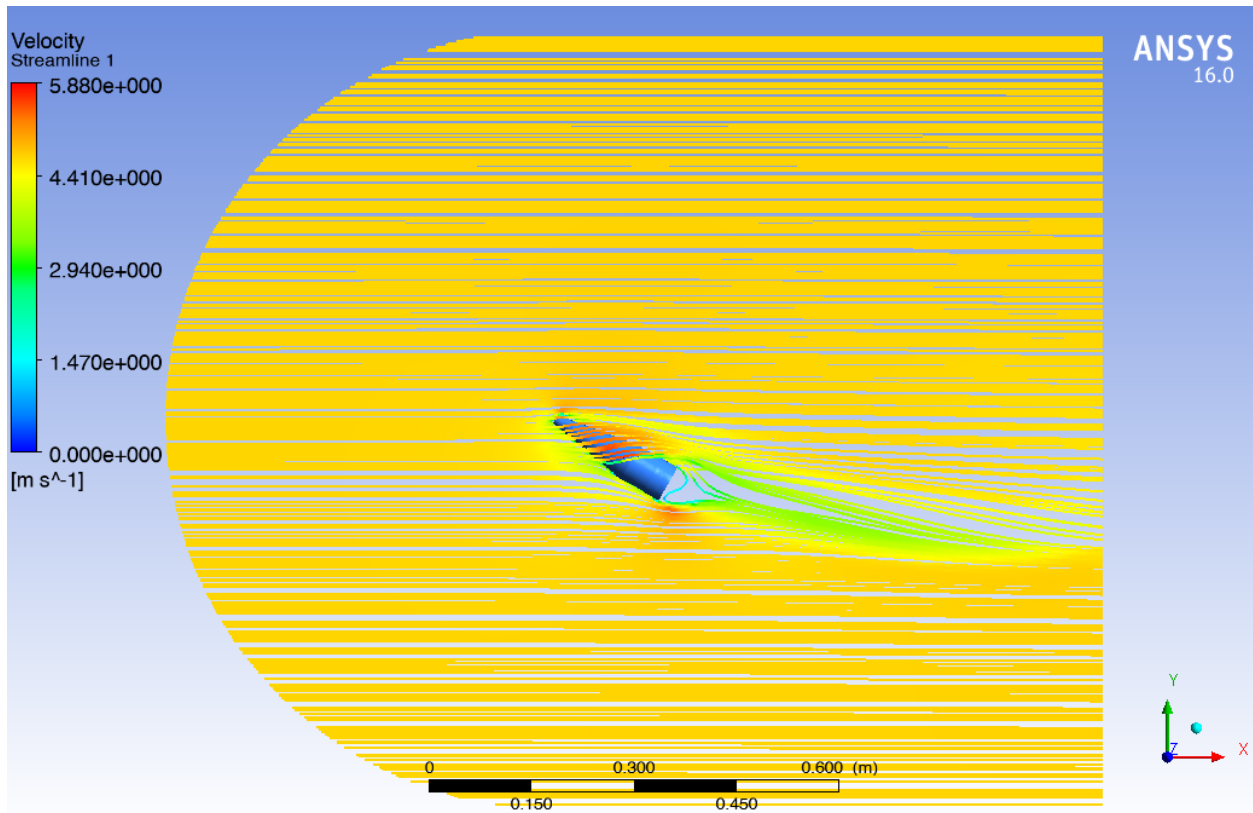


Figure 27 : The velocity contour for 57 mm projectile at 45°AOA.

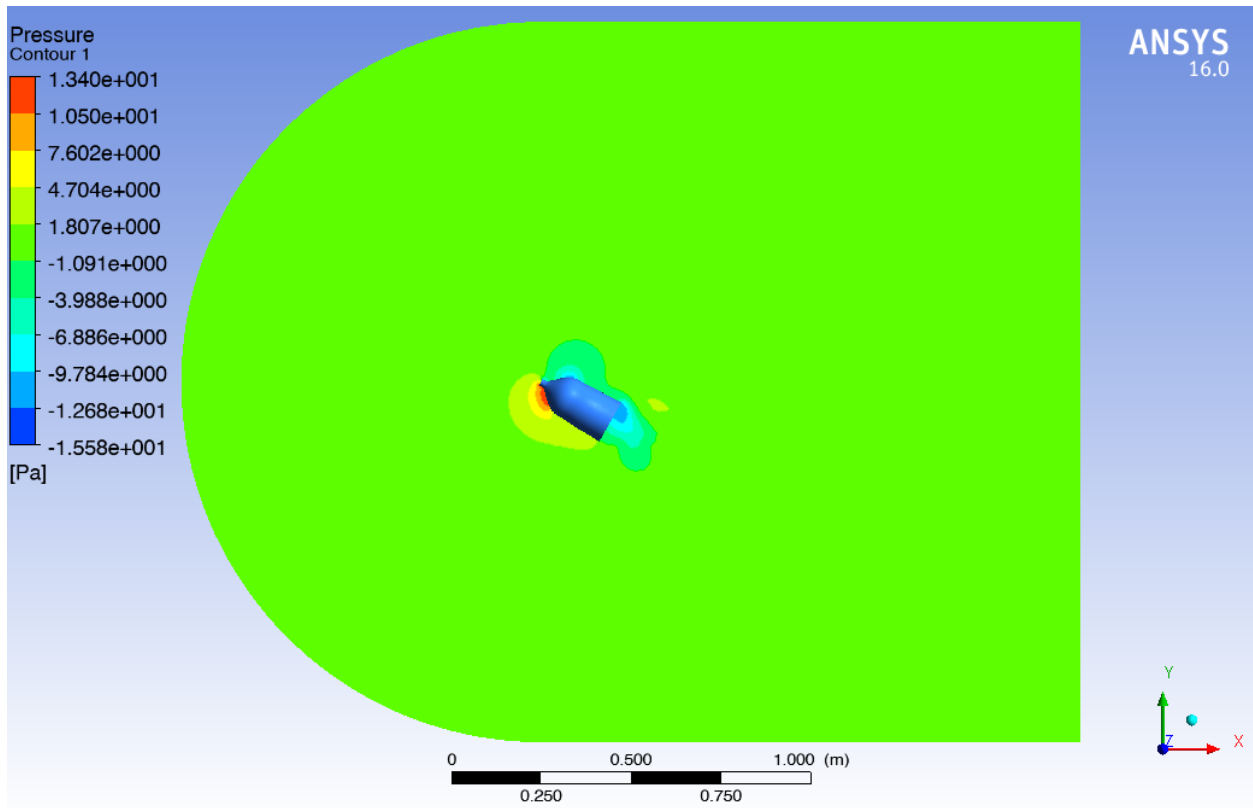


Figure 28 : The pressure contour for 125 mm projectile at 45°AOA.

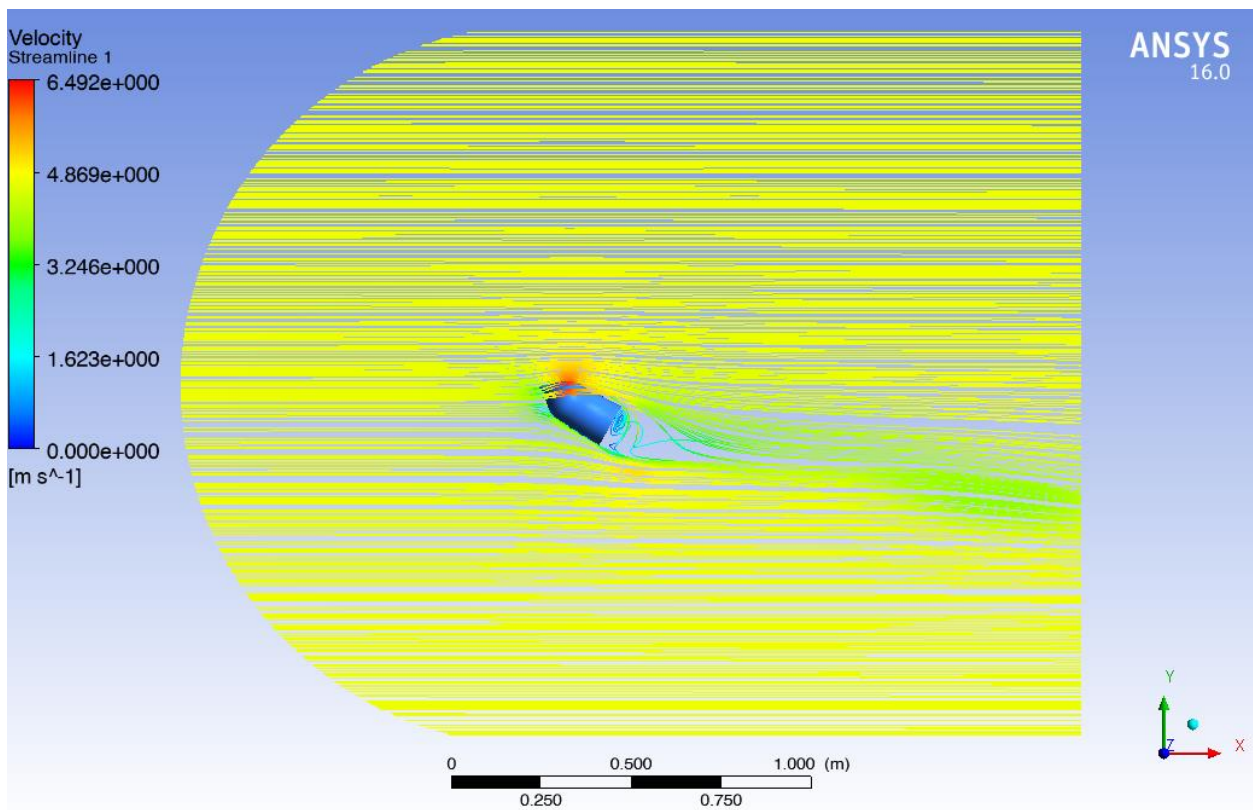


Figure 29 : The velocity contour for 125 mm projectile at 45°AOA.

5.4 Simulation at Higher Speed

A supersonic simulation was done to investigate the drag and lift forces. The simulation in supersonic speed is not the same as the subsonic speed therefore the comparison of the simulation result was different. However, the trend was familiar as the lift and drag coefficient changes near our Experimental speed is almost negligible.

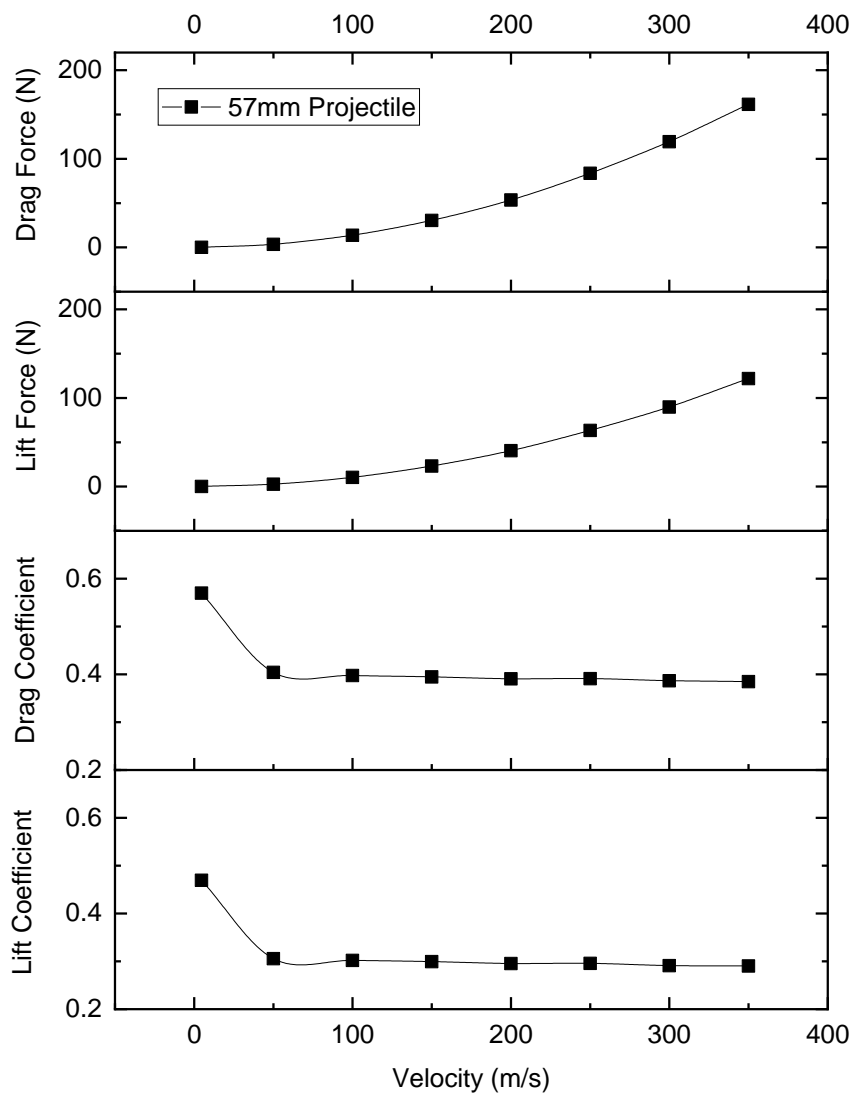


Figure 30 : The lift and drag coefficient of 57 mm projectile at 45° AOA for supersonic speed.

5.5 Results in different Orientation

An additional set of experiments was conducted for 57 mm. The projectile was rotated at a different angle corresponding to the vertical axis while keeping the projectile at 45° angle corresponding to the horizontal axis. Figure 31 shows the rotation of the projectile relative to the vertical axis. The projected area was calculated through SolidWorks. Mathematically, the Left and Right side have the same projected area as the projectile is symmetric. Figure 32 shows the projected area for the Side, 45° Left, and Back of the projectile. The Experimental results are shown in Figure 33 and the related data is shown in Table 7. The total forces acting on the projectiles are highest for the side orientation (90 Degree) as the physical size is the largest from this angle. The minimum forces observed from the front. The total projected area is less for 45° angle compare to the 0° angle and the total force acting on the projectile is increase. The reason is, the total number of measurable strips were less. Some areas of the projectile were visible but there was not tapping point, therefore the suction force was less at measurable tapping and hence increased the total force. In aerodynamics study, the pressure on the curved surfaces is measured with an array sensor the density of the array sensor increases the precision of the measurement. The forces acting in the back could be working in favor of the projectile range due to the combined effect of the attack angle of the wind, orientation of the projectile. The back of our projectile was hollow and there was no tapping point, therefore the experimental total forces are very dependable in this case.

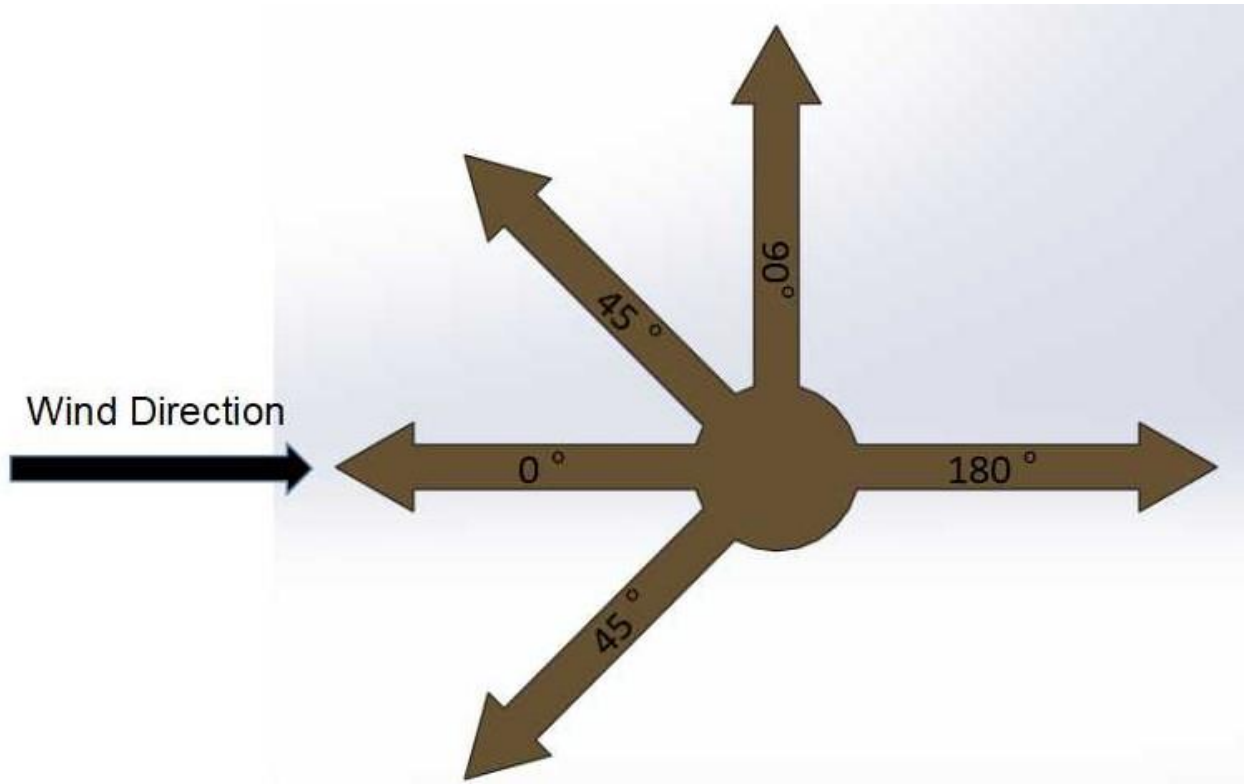
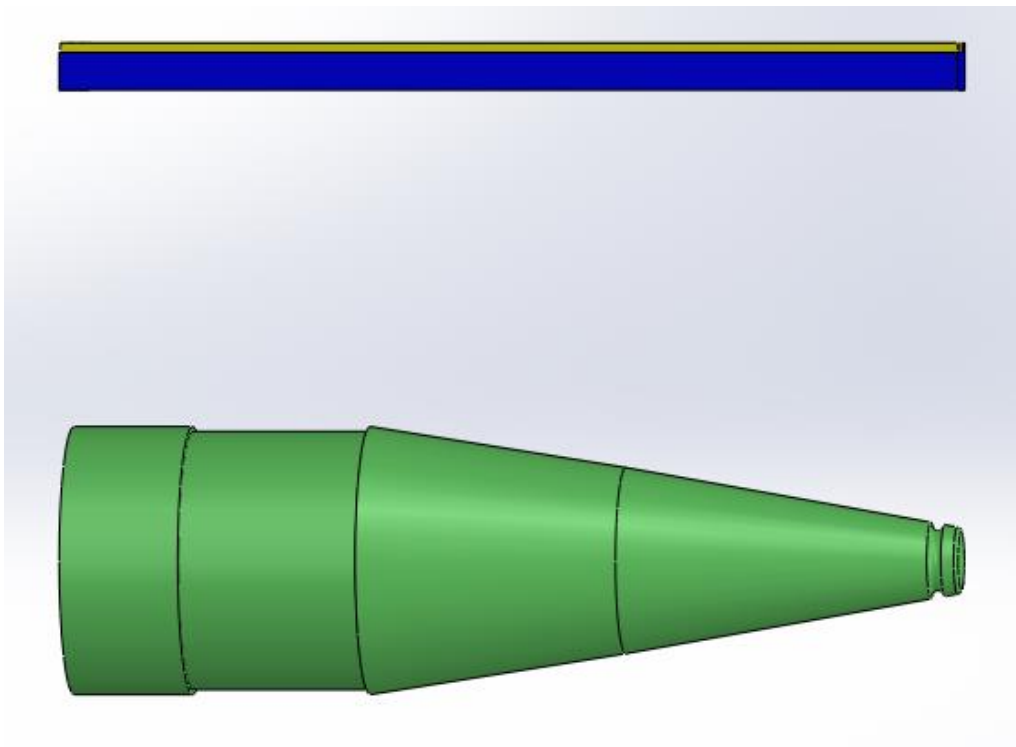
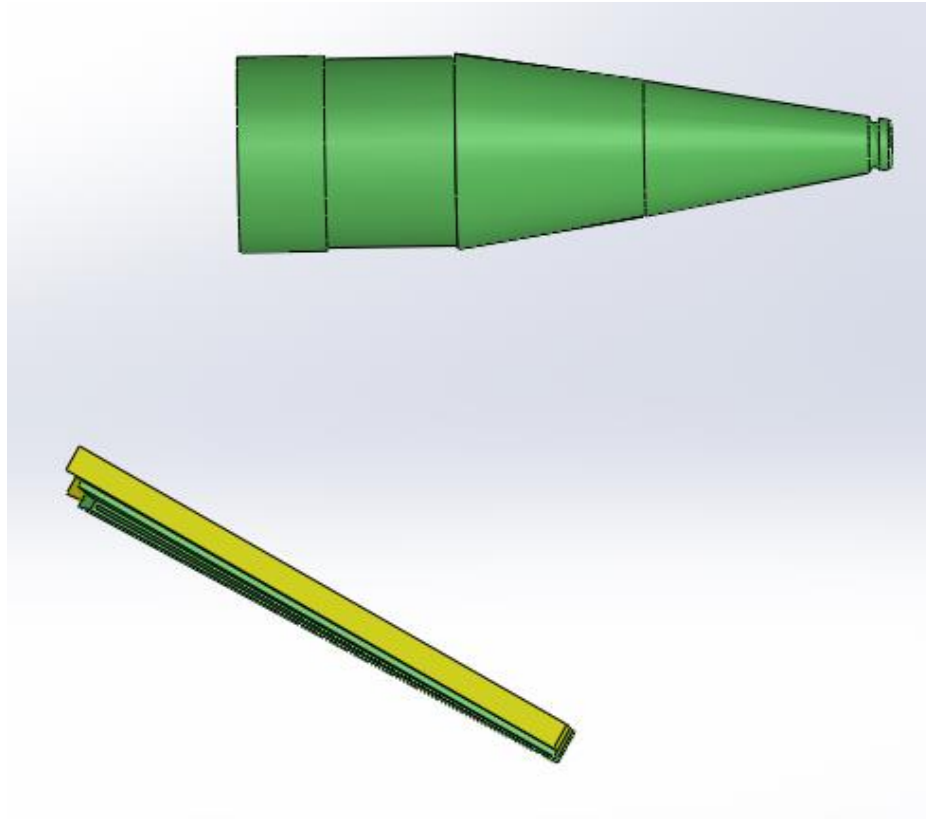


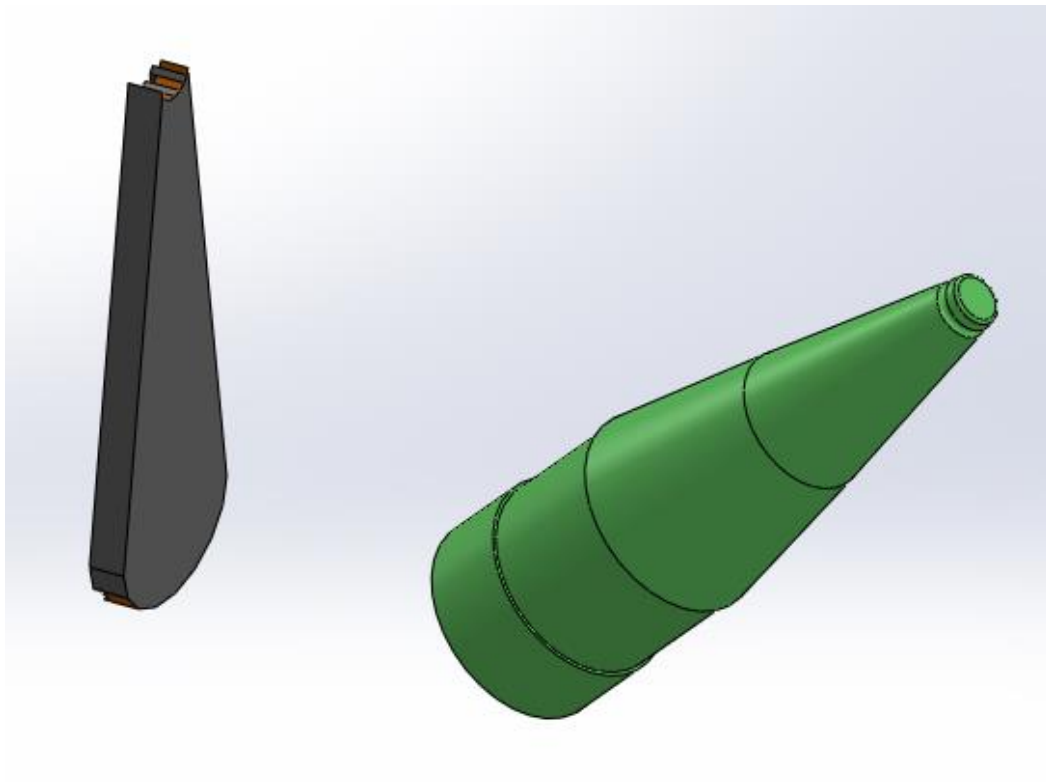
Figure 31: The rotation of the 57mm projectile at different angles.



(a)

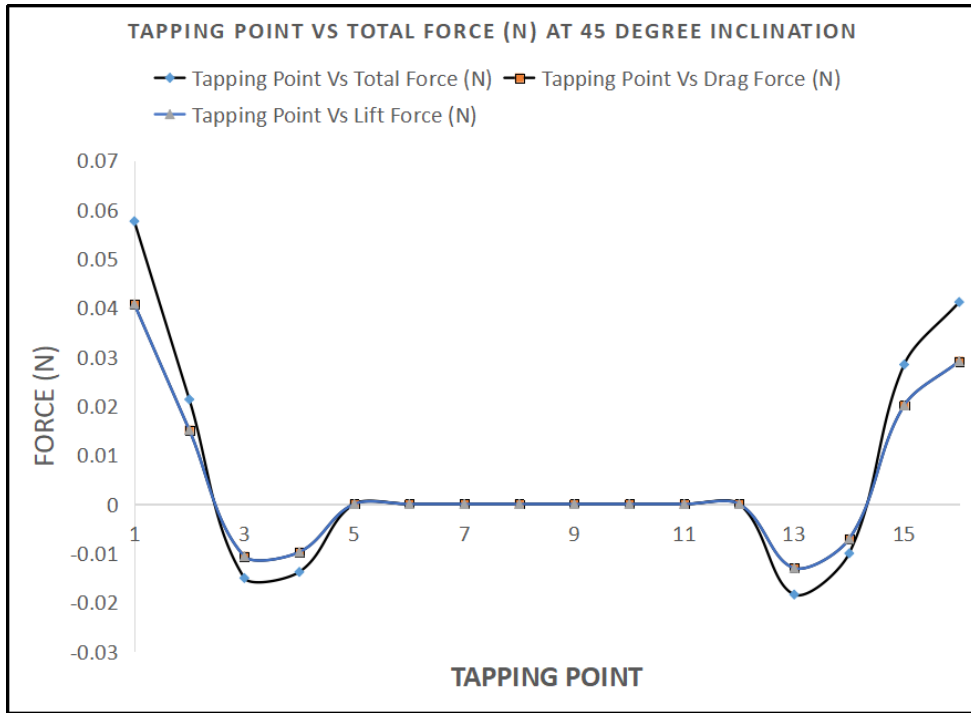


(b)

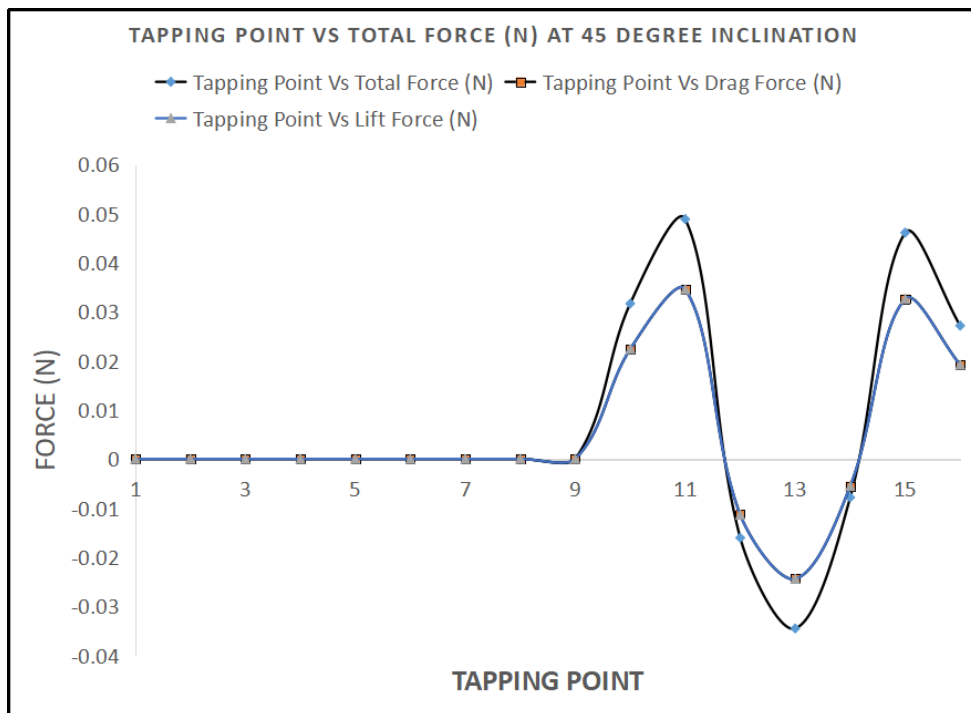


(c)

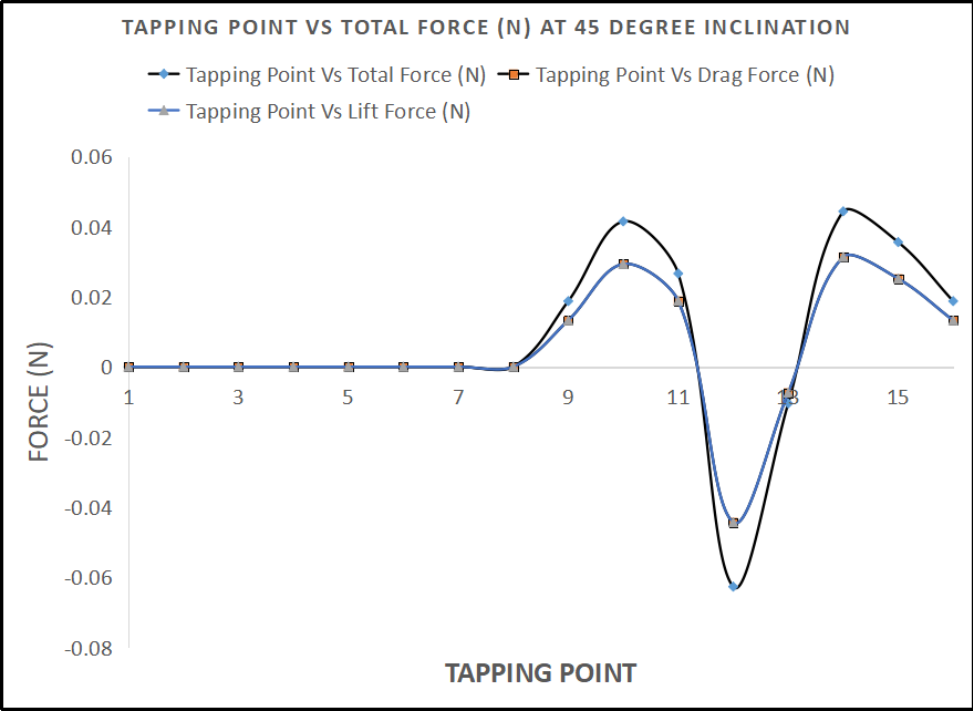
Figure 32 : The projected area for (a) Side (b) 45 Degree Left, and (C) Back



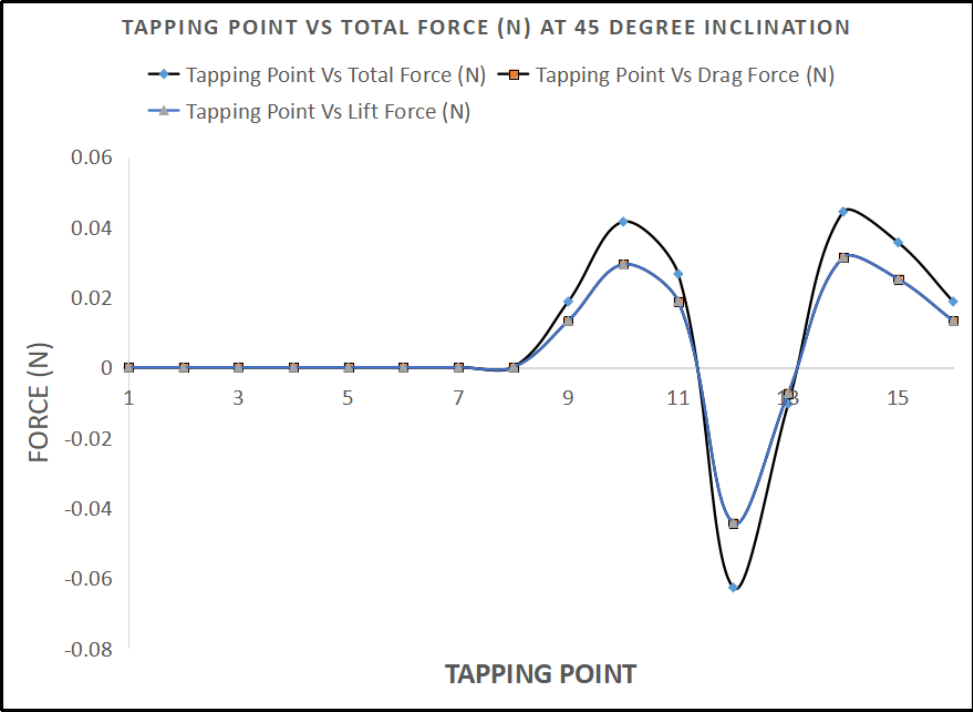
(a) 0° Location (Original Location)



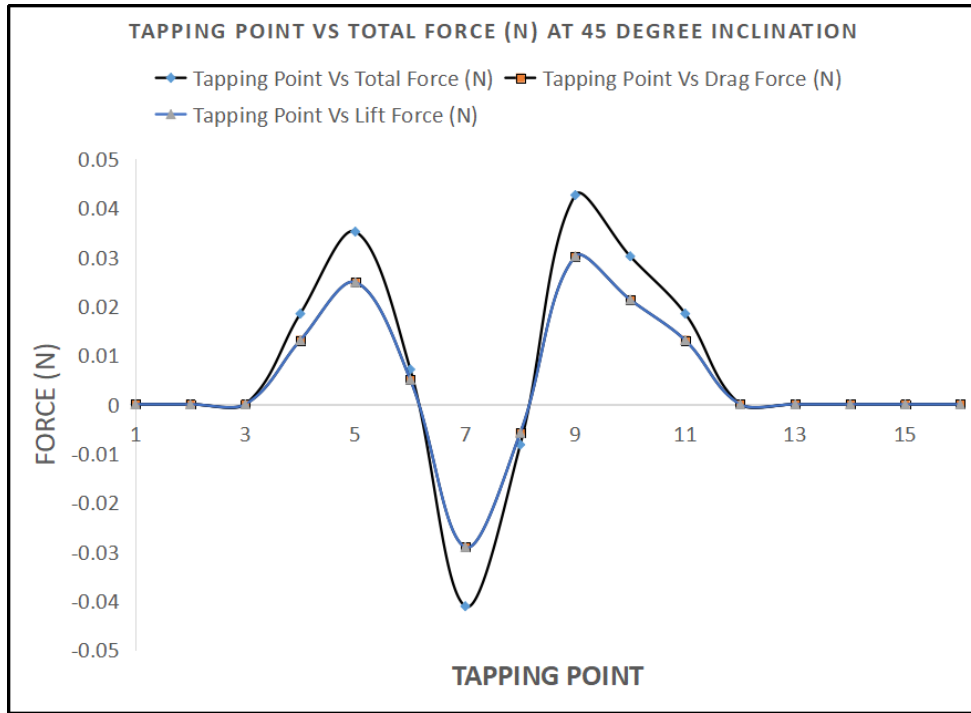
(b) 45° Left



(C) 45° Right



(D) 90° Side



(E) Back (180°)

Figure 33 : Forces acting on the Projectile at different 45° at a different orientation.

Table 7: Total acting forces on 57 mm Projectile at 45° attack angle and for different orientations.

Test Condition	Projected Area (m ²)	Total Force (N)
Side (90 Degree)	0.0067452	0.112139235
Oblique Right (45 Degree)	0.00521594	0.098521677
Oblique Left (45 Degree)	0.00521594	0.095288481
Back (180 Degree)	0.00559558	0.091064169
Front (Original 0 Degree)	0.00559529	0.091064169

CHAPTER- 6

CONCLUSION AND RECOMMENDATION

6.1 Conclusion

The projectile flies at supersonic speed and not in subsonic speed. This study allows observing the projectile behavior at low speed. The projectile starts at zero velocity, therefore, the experiment that is conducted at 4.7 m/s provides the initial flight scenario and the drag force and lift forces related to it. The experimental and simulation process developed in this thesis can be used to investigate the projectiles at supersonic speed.

The findings of this research are as follows:

- a. The drag and lift forces are found to be the function of the projectile sizes. For the same angle of attack (say 50°), the drag forces for 37, 57, and 125 mm projectile are 0.0224 N, 0.0492 N, and 0.1629N. The lift force also increases (0.0159 N, 0.0382 N, and 0.1296 N) but the rate of increasing the lift forces is more than the drag forces (For Drag Force, 54.4% (57) and 86.2% (125), For Lift Force, 58% (57) and 87.87% (125)). Therefore, a large size projectile may have large drag but due to size, the lift force increases too.
- b. The lift and drag forces are also a function of the Angle of Attack (AOA). The lift and drag forces increase as the angle of attack increases from 30° to 50° . The trend of the increase is found to be linear for subsonic airspeed. The rate of increasing the lift forces is higher (45% for 57 mm Projectile, calculated from the slope of the curve fitting) than the drag force.
- c. The lift and drag coefficients are related to the lift and drag forces. Therefore, they follow a similar trend with AOA for drag and lift forces.
- d. The pressure coefficients are positive at some tapping points of the projectile and the tapping points move away from the center. The airflow creates a

vacuum to the tapping points away from the center and hence the manometer fluid provides negative pressure.

- e. The simulation shows the pressure contour for different projectiles and all the pressure contour Figures show that the maximum pressure is generated at the front where the air hits. This result validates the experimental findings where it was observed that the manometers at the front tapping points provide positive displacement and as the tapping points move away from the front the manometer deflection reduces gradually and after some point, it deflects the other way due to the negative pressure.

We have carried out our experiment in wind tunnels which may have underestimation of crosswind effects and model preparation also could not be done very accurately for that the experimental and simulation results show some deviation.

6.2. Recommendations

For the smooth conduct of the thesis and also for subsequent study on a similar topic following recommendation are made:

- (a) The manufacturing of the projectiles model should be done with metal in CNC lathe to get realistic and more accurate results.
- (b) The experiment should have been done in supersonic wind tunnel to get precision measurement.
- (c) The precision of the measurement could be increased with flat skin sensors.
- (d) Experiment should be focused on a single projectile rather than multiple projectiles, to have in-depth study on it.
- (e) The flow behaviour around the projectile and effect of Reynolds number may be taken into consideration.
- (f) In future along with the study of aerodynamic characteristics, the design parameter of the projectiles should be studied to have scope of redesigning the projectile with optimized parameters.

REFERENCES

7. References

- [1] Mohammad, A. D. Slobodan, J. (2018), " Various Methods of Artillery Projectiles Base Drag Reduction", 8th International Scientific Conference on defence Technology Belgrade, Serbia.
- [2] Elsaadany, A. Wenjun Yi. (2014), "Investigation on Trajectory Correction for Typical Artillery Projectiles", 5th International conference on Mechanical Engineering and Mechanics, China.
- [3] Mahfouz, E. W. Zhengui, H. Zhihua, C. (2014), "Aerodynamic Characteristics and Flow Field Investigations of an Optimal Hollow Projectile". 5th International Conference on Mechanical Engineering and Mechanics, China.
- [4] Torangatti, K. Basawaraj, (2014), "Drag Prediction and validation of Standard M549, 155mm Projectile", International journal of Engineering Research and Reviews, India, vol. 2, Issue 3, pp. 26-32.
- [5] Sasar, R. B. Naik, S. D. (2013), "Drag Brakes Variation for Range Correction of Artillery Projectile", International Journal, India, vol. 2, Issue 9.
- [6] Baranowski, L. Godomski, B. Majewski, P. Szymonik, J. (2018) "The Analysis of the 35 mm Artillery Projectile's Motion Model Parameters' Identification Based on the Recorded Flight Trajectory", 24th International conference on Engineering Mechanics, Czech Republic, pp. 53-56.
- [7] Suliman, M. A. Mahmoud, O. K. Sanabawy, M. A. Abdel, O.E. (2009), "Computational Investigation of Base Drag Reduction for a Projectile at Different Flight Regimes", 13th International Conference on Aerospace Science and Aviation technology Coiro, Egypt.
- [8] Alexandar, B. (2013), "Long Distance Bullets and Shells", International Journal of Aerospace Science, Brooklyn, USA, vol. 2, Issue 2, pp. 29-36.
- [9] Chand, K. K. Pattnaik, S. (2008), "Modeling Projectile Motion: A System Dynamics Approach", International Journal on Information Science and Computing Orissa, India, vol. 2, No.1.

- [10] Goran, J. O. Bosko, P. R. Aleksandar, C. B. (2017), "Aerodynamic Shape Optimization of Guided Missile Based on Wind Tunnel Testing and Computational Fluid Dynamics Simulation", Serbia, Scientific Paper, vol. 21, No. 3, pp. 1543-1554.
- [11] Liang, K. Zheng, H. Jing, M. Z. (2017), "Optimal Design of the Aerodynamic Parameters for a supersonic Two-Dimensional Guided Artillery Projectile", Article on Defence Technology, vol. 13, pp. 206-211.
- [12] Chand, K. K. Panda, H. S. (2007), "Mathematical Model to Simulate the Trajectory Elements of an Artillery Projectile Proof Shot", Defence Science Journal, India, vol. 57, No. 1, pp. 139-148.
- [13] Ahmed, F. M. K. (2009), " Numerical Computations of Transonic Critical Aerodynamic Behavior of a Realistic Artillery Projectile", Engineering Journal, Iraq, vol. 5, No. 1, pp. 42-52.
- [14] Sahoo, S. Laha, M. K. (2014), "Coefficient of Drag and Trajectory Simulation of 130 mm Supersonic Artillery Shell with Recovery Plug of Fuze", Defence Science Journal, India, vol. 64. No. 6. pp. 502-508.
- [15] Elya, C. Amy, C. Michael, C. (2014) "Experimental Tests of the Proportionality of Aerodynamic Drag to Air Density for Supersonic Projectiles," International Article, USA.
- [16] Jian, S., Shaobo, F. Yaxin, J. Zhu, Q. Duan, J. (2020), "Aerodynamics Analysis of a Hypersonic Electromagnetic Gun Launched Projectile", Journal Pre-Proof, China, Ref. DT 592.
- [17] Jaswinder, S. Jaswinder, S. Ampritpal, S. Abhishek, R. Ajay, D. (2015), "Study of NACA 4412 and Selig 1223 Airfoils Through Computational Fluid Dynamics", International Journal, India, vol. 2, Issue 6.
- [18] Shane, M. (2009), " That's a Drag: The Effects of Drag Forces", Journal of Mathematical Modeling, USA, vol. 2, Issue 1, Article 4.
- [19] Shubnam, J. Nekkanti, S. Sriram, K. (2015), "Effect of Reynolds Number on Aerodynamics of Airfoil with Gurney Flap", International Journal of Rotating Machinery, India, vol.2015, 2015.
- [20] Wenjun, Y. Dongyang, S. Junjie, T. Dandan, Y. (2012), " Experimental Research on Aeroelasticity of a Large Length to Diameter Ratio Projectile", International Journal of Modern Physics of Fluid, China, vol. 19, pp. 270-275.

- [21] Peter, C. (2014), "Approximate Analytical Description of the Projectile Motion with a Quadratic Drag Force", Athens Journal of Science, Russian Federation, vol. 1, No. 2, Issue 2, pp. 97-104.
- [22] Mariusz, M. Tomasz, M. (2017), "Comparison Analysis of Drag Coefficients for Supersonic Mortar Projectiles", International Journal, Poland, vol. 140, No. 4/2016, pp. 21-28.
- [23]. Hossam, A.A.E.M. Osama, M.K.M.M. (2015), "Study of the Aerodynamics of Extended Range of Artillery Projectile with Base Bleed and Rocket Assistance", Thesis for PhD, Cairo, Egypt.
- [24] Damir, D.J. Marija, S. (2008), "The Aerodynamic Characteristics Determination of Classic Symmetric Projectile", 5th International Symposium about forming and design in Mechanical Engineering, Serbia.
- [25] Tong, Z. Xiaoli, Z. Zhendong, S. (2014), "Aerodynamic Characteristic Analysis of Two-Dimensional Trajectory Corrector Projectile in Mortar", Technical Publication on Applied Mechanics and Materials, China, vol. 624, pp. 236-239.
- [26] Jiemin, L. Guanglin, H. Haoyang, G. (2015), " A Study on the Aerodynamic Characteristics for a Two-Dimensional Trajectory Correction Fuze", Tech Publication, China, vol. 703, pp. 370-375.
- [27] Jan, K. F. Shen, M. L. (2007), "Numerical Study of Base Bleed Effects on Aerodynamic Drag For A Transonic Projectile", Taiwan. China, International Journal on Computational Fluid Dynamics, China, vol. 1, Issue. 3, pp. (249-273).
- [28] Hruschka, R. Klatt, D. (2019), "In-Pipe Aerodynamic Characteristics of a Projectile is Comparison With Free Flight For Transonic Mach Numbers", International Journal, France, vol. 29, pp. 297-306.
- [29] Chun, C. L. Chang, S. T. Cheng, C. L. Yen, C. T.(2014), "Study of The Aerodynamic Characteristic And Flight Trajectories in a Tail Fin-Stabilized Projectile With Different Shapes", 1st International Conference on Mechanics , China, Procedia Engineering 79, pp. 108-113, 2014.
- [30] Lai, H. C. Kamaruddin, N. M. (2018), "Effect of Fuselage Diameter on Aerodynamic Characteristics for Straight Wing at Low and High Aspect Ratio", International Conference

on Aerospace and Mechanical Engineering (Aero Mech 17), IOP Conference Series Mater. Sci.Eng. 370, 012055.

[31] Ahmed, E. Yi, W. J. (2014), "Accuracy Improvement Capability of Advanced Projectile Based on Course Correction Fuze Concept", The Scientific World Journal, China, vol. 2014, Article ID 273450.

[32] Tyler, B. Semih, M. O. (2014), "Experimental Study on The Effects of Nose Geometry on Drag Over Axisymmetric Bodies in Supersonic Flow", Thesis Paper for MSc degree, USA.

[33] Tolga, D. Firat, B. Utlü, C. (2017), "A Review of Gun Barrel Vibration and Control for a Main Battle Tank ", International Journal on defence technology 13, Turkey, pp. 353-259.

[34] Sangeeta, S. P. Gite, L. K. Anandaraj, A. Rajan, K. M. (2017), "Dispersion Sensitivity Analysis & Consistency Improvement of APFSDS", International Journal on defence Technology 13, India, pp. 316-322.

[35] Magier, M. (2010), "The Conception of The Segmented Kinetic Energy Penetrators for Tank Guns", International Journal of applied Mechanics, Poland, vol. 77.

[36] Motyl, K. Magier, M. Zygmunt, B. (2017), "Theoretical and Experimental research of Anti Tank Kinetic Penetrator Ballistics", Bulletin of Polish Academy, Poland, vol. 65 No. 3.

[37] Alexey, M.L. Stanishlav, A.K. Ivan, G.R. (2017), "Optimization of Aerodynamic Form of Projectiles for Solving the Problem of Shooting Range Increasing", AIP Conference Proceeding 1893, 030085.

[38] Hemateja, A. Ravi, B. Teja, A. Dileep, K. Rakesh, S.G. (2017), "Influence of Nose Radius of Blunt Cones on Drag in Supersonic and Hypersonic Flows", Material Science and Engineering, Vol. 225, 012045.

APPENDIX

8.1 Appendix A

Inclined Multi-Manometer reading of 37 mm Projectile

Manometer Number	Initial h_1 (mm)	30° (h_2 , mm)	35° (h_2 , mm)	40° (h_2 , mm)	45° (h_2 , mm)	50° (h_2 , mm)
1	142	135	139	137	138	138
2	142	148	148	145	146	146
3	142	153	150	147	148	148
4	142	145	145	145	147	145
5	142	147	147	146	146	147
6	142	143	143	145	144	143
7	142	143	143	147	144	143
8	142	152	150	149	149	149
9	142	150	148	147	145	145
10	142	134	139	139	139	135

8.2 Appendix B

Inclined Multi-Manometer reading of 57 mm Projectile

Manometer Number	Initial h_1 (mm)	30° (h_2 , mm)	35° (h_2 , mm)	40° (h_2 , mm)	45° (h_2 , mm)	50° (h_2 , mm)
1	142	132	135	135	135	134
2	142	138	138	139	139	137
3	142	152	150	143	145	146
4	142	154	154	149	148	151
5	142	145	140	145	151	141
6	142	159	150	143	149	149
7	142	151	151	144	155	147
8	142	148	140	146	158	148
9	142	149	147	144	155	149
10	142	162	151	149	159	149
11	142	146	139	145	160	141
12	142	151	148	148	152	150
13	142	152	152	154	150	149
14	142	145	144	146	144	147
15	142	139	137	137	138	138
16	142	136	136	136	137	136

8.3 Appendix C

Inclined Multi-Manometer reading of 125 mm Projectile

Manometer Number	Initial h_1 (mm)	30° (h_2 , mm)	35° (h_2 , mm)	40° (h_2 , mm)	45° (h_2 , mm)	50° (h_2 , mm)
1	142	135	133	130	130	131
2	142	137	134	135	132	136
3	142	139	137	138	135	140
4	142	141	148	143	138	141
5	142	145	151	145	153	147
6	142	148	152	148	157	149
7	142	153	151	150	158	150
8	142	151	151	151	152	151
9	142	155	153	150	146	150
10	142	148	146	149	150	150
11	142	153	155	148	149	149
12	142	152	158	152	154	148
13	142	146	146	153	154	147
14	142	150	150	152	153	150
15	142	151	149	153	152	149
16	142	149	147	154	153	148
17	142	145	146	155	148	150
18	142	149	149	155	155	148
19	142	150	150	154	153	151
20	142	154	154	152	154	150
21	142	148	148	145	155	148
22	142	153	151	146	152	150
23	142	151	151	151	156	152
24	142	150	150	148	155	150
25	142	144	144	147	153	149
26	142	141	140	146	145	145
27	142	139	137	141	135	139
28	142	138	135	137	133	135
29	142	136	133	134	132	132
30	142	135	130	132	131	130

8.4 Appendix D

Inclined Multi-Manometer reading of 57 mm projectile in Oblique Angles

Manometer Number	Initial h_1 (mm)	45° Degree Left (h_2 , mm)	45° Degree Right (h_2 , mm)	45° Degree Side (h_2 , mm)	180° (h_2 , mm)
1	13	15	15	13	15
2	13	16	14	14	14
3	13	14	4	16	12
4	13	12	4	15	5
5	13	15	15	14	6
6	13	14	17	16	12
7	13	16	14	14	18
8	13	15	5	13	14
9	13	11	3	4	7
10	13	3	14	6	7
11	13	5	14	10	5
12	13	15	15	19	15
13	13	17	17	14	14
14	13	14	16	8	12
15	13	5	14	7	11
16	13	3	13	4	10